

This is the author's peer reviewed, accepted manuscript. However, the online version of record will be different from this version once it has been copyedited and typeset.

PLEASE CITE THIS ARTICLE AS DOI: 10.1063/5.0079883

Revised manuscript

### Molecular modeling of the interface of an egg yolk protein-based emulsion

Marco Ferrari,<sup>1</sup> Jan-Willem Handgraaf,<sup>2</sup> Gianluca Boccardo,<sup>1</sup> Antonio Buffo,<sup>1, a)</sup> Marco Vanni,<sup>1</sup> and Daniele L. Marchisio<sup>1</sup>

<sup>1</sup>*Department of Applied Science and Technology, Politecnico di Torino, Corso Duca degli Abruzzi 24, 10129, Torino, Italy*

<sup>2</sup>*Siemens Industry Software Netherlands B.V., Galileiweg 8, 2333 BD, Leiden, The Netherlands*

(Dated: 4 January 2022)

Many food emulsions are stabilized by functional egg yolk biomolecules, which act as surfactants at the oil/water interface. Detailed experimental studies on egg yolk emulsifying properties have been largely hindered due to the difficulty in isolating individual chemical species. Therefore, this work presents a molecular model of an oil/water interfacial system where the emulsifier is one of the most surface-active proteins from the egg yolk low-density lipoproteins (LDL), the so-called Apovitellenin I. Dissipative Particle Dynamics (DPD) was here adopted in order to simulate large systems over long time-scales, when compared with full-atom molecular dynamics (MD). Instead of a manual assignment of the DPD simulation parameters, a fully-automated coarse-graining procedure was employed. The molecular interactions used in the DPD system were determined by means of a parameter calibration based on matching structural data from atomistic Molecular Dynamics (MD) simulations. Despite of the little availability of experimental data, the model was designed to test the most relevant physical properties of the protein investigated. Protein structural and dynamics properties obtained via MD and DPD were compared highlighting advantages and limits of each molecular technique. Promising results were achieved from DPD simulations of the oil/water interface. The proposed model was able to properly describe the protein surfactant behavior in terms of interfacial tension decrease at increasing protein surface concentration. Moreover, the adsorption time of a free protein molecule was estimated and, finally, an LDL-like particle adsorption mechanism was qualitatively reproduced.

---

<sup>a)</sup> Author to whom correspondence should be addressed: antonio.buffo@polito.it

This is the author's peer reviewed, accepted manuscript. However, the online version of record will be different from this version once it has been copyedited and typeset.

PLEASE CITE THIS ARTICLE AS DOI: 10.1063/1.50079883

## 1 I. INTRODUCTION

2 Food emulsions are made of a continuous water phase, a disperse phase with a high content  
3 of oil, and a surfactant that stabilizes the oil drops.<sup>1-5</sup> The droplet size distribution (DSD)  
4 is the most important property of the emulsion since the structure, stability, taste, and  
5 color of the final product depend on the DSD.<sup>1-5</sup> The DSD in turn depends on the emulsion  
6 composition, the type of process and the operating conditions under which the production  
7 process operates.<sup>6</sup> The production of emulsions is based on mixing the ingredients and  
8 applying a suitable mechanical energy to the emulsion for promoting droplet formation and  
9 breakage, in order to reach the desired DSD. A typical mixing process is composed by two  
10 steps: first, the ingredients (mainly egg yolk, vinegar, oil, water, salt) are mixed together in  
11 large stirred vessels at moderate rotational speed; then, this premixed emulsion is fluxed into  
12 a high-shear device, commonly a cone mill mixer, where the oil droplets undergo breakage  
13 until the final size distribution is reached.<sup>3-5</sup> This last step is crucial to fine-tune the DSD,  
14 in order to determine the properties of the final product.

15 Many food emulsions are stabilized by surface-active biopolymers that adsorb on the  
16 droplet surface and form protective coatings.<sup>1</sup> Some of these functional molecules are integral  
17 components of more complex food ingredients used in food products (e.g., egg yolk, milk, and  
18 flour).<sup>1,2</sup> Although the egg yolk is recognized as one of the most widely employed emulsifiers  
19 for both industrial and home-made food emulsion preparation,<sup>1</sup> many issues need to be  
20 addressed, especially the adsorption mechanism of egg yolk proteins at oil-water interface  
21 and their emulsifier behaviour.<sup>7</sup> Indeed, the egg yolk is a complex system with different  
22 structural levels consisting in non-soluble protein aggregates (granules) in suspension in  
23 a clear yellow fluid (plasma) that contains low-density lipoproteins (LDLs) and soluble  
24 proteins.<sup>7</sup> Experimental research concerning the emulsifying properties of egg yolk proteins  
25 has been hindered by the difficulties in extracting individual components from the complex  
26 matrix, therefore, they are less amenable to detailed study by being less readily available in  
27 pure form.<sup>8-10</sup>

28 During the emulsification process, the interfacial properties between disperse and contin-  
29 uous phases play an essential role in the formation and the stabilization of the oil droplets.<sup>1,2</sup>  
30 Therefore, it is important to have a fundamental understanding of the factors that influ-  
31 ence the type, concentration, interactions, and arrangement of surface-active molecules at

This is the author's peer reviewed, accepted manuscript. However, the online version of record will be different from this version once it has been copyedited and typeset.

PLEASE CITE THIS ARTICLE AS DOI: 10.1063/1.50079883

32 interfaces.<sup>1,2</sup> Computer modeling techniques can greatly enhance the comprehension of the  
33 way the molecules organize themselves in a liquid.<sup>11–14</sup> Molecular simulations can provide  
34 valuable insight into the relationship between molecular properties and structural organiza-  
35 tion that are relevant for a better understanding of the behavior of food emulsions, including  
36 the miscibility/immiscibility of liquids, the formation of surfactant micelles, the adsorption  
37 and displacement of emulsifiers at interfaces, the transport of nonpolar molecules through  
38 aqueous phases, the conformation and flexibility of biopolymers in solution, polymer inter-  
39 actions, and the formation of gels.<sup>15–24</sup> The first step in a molecular simulation is to define  
40 the characteristics of the molecules involved (e.g., size, shape, flexibility, and polarity) and  
41 the nature of the intermolecular pair potentials that act between them, making a number  
42 of simplifying assumptions as a compromise between the model reliability and a reasonable  
43 computational time.<sup>25</sup> A collection of these molecules is arbitrarily distributed within a box  
44 that represents a certain region of space, and the change in the conformation and/or orga-  
45 nization of the molecules is then monitored as they are allowed to interact with each other.  
46 Depending on the simulation technique used, one can obtain information about the evolution  
47 of the structure with time and/or about the equilibrium structure of the molecular ensem-  
48 ble. The most commonly used computer simulation techniques in this context are the Monte  
49 Carlo approach and Molecular Dynamics (MD). In these models the involved molecules can  
50 be described with all their atomistic details or some of them can be coarse-grained, as in  
51 Dissipative Particle Dynamics (DPD).<sup>19,26–30</sup>

52 Many molecular modeling studies of food structures were carried out employing the afore-  
53 mentioned approaches.<sup>19</sup> The adsorption of flexible proteins ( $\beta$ -casein<sup>31</sup> and a proteinlike  
54 heteropolymer<sup>32</sup>) at an oil-water interface was studied by means of Monte Carlo simula-  
55 tions. On the other hand, the majority of MD studies on protein adsorption at fluid inter-  
56 faces have been on globular proteins using both all-atom and coarse-grained models, with  
57 few studies on unstructured intrinsically disordered proteins.<sup>33–40</sup> Few works have been car-  
58 ried out on protein models via coarse-grained DPD technique, although this approach allows  
59 the simulation of large systems over relatively long-time scales with respect to full-atomistic  
60 studies.<sup>28,29,41</sup> DPD uses simplified soft potentials and coarse-grained representations of mod-  
61 eled structures.<sup>27–29</sup> In contrast to MD, in DPD systems the intended physical properties are  
62 determined by means of parameter calibration. One of the most popular method of calibra-  
63 tion is based on mapping onto Flory–Huggins theory.<sup>29</sup> Another approach is to couple DPD

This is the author's peer reviewed, accepted manuscript. However, the online version of record will be different from this version once it has been copyedited and typeset.

PLEASE CITE THIS ARTICLE AS DOI: 10.1063/1.50079883

64 with MD simulations to calibrate models by matching the structural data from the atomistic  
65 simulations.<sup>42-44</sup> Previous DPD studies investigated the adsorption of semi-flexible rod-like  
66 objects,<sup>45</sup> conformation changes<sup>46</sup> or the folding of small proteins.<sup>47</sup> However, all computer  
67 molecular techniques have been successfully employed in modeling of interfacial systems and  
68 in the calculation of the surface tension when an amphiphilic non-protein molecule act as a  
69 surfactant.<sup>48-51</sup> Moreover, DPD is well-suited for modeling of multi-component systems such  
70 as emulsions, and it has been used in a number of studies to look at the effect of adsorbing  
71 molecules on the stability of oil or water droplets in emulsions.<sup>19,52-54</sup> These have mainly  
72 been carried out on hydrocarbon oil emulsions with synthetic copolymers as the adsorbing  
73 molecules, but the methodology and the general results are relevant also for food emulsions.

74 The main goal of the present work is to model an oil/water interfacial system where  
75 the emulsifier is one of the most surface-active proteins from the egg yolk LDL, in order to  
76 provide new insights into physics of the food emulsion production process. Despite of the  
77 little availability of experimental data, the model was designed to test the most relevant  
78 physical properties of such a protein by means of the DPD approach in which the parameter  
79 calibration is based on MD simulations. Instead of a manual assignment, a fully *automated*  
80 coarse-graining procedure was employed to the molecules involved in the ternary system,  
81 assuming a flexible, disordered structure for the protein. Promising results were obtained  
82 in terms of both equilibrium and dynamic properties of the egg-yolk protein. Finally, the  
83 adsorption mechanism of a LDL-like particle is also qualitatively reproduced.

84 This paper is structured as follows: in Section II the molecular description of the studied  
85 system is presented; the molecular techniques here used are briefly introduced in Section  
86 III; the model development and calibration are explained in Section IV together with all the  
87 simulation details; Section V shows the relevant results of systems investigated and, finally,  
88 in Section VI the main conclusions are reported.

## 89 II. MOLECULAR DESCRIPTION OF THE MACROSCOPIC SYSTEM

90 The first step in the development of the molecular model for an egg yolk protein-based  
91 emulsion is to identify the chemical species to be simulated and to define the characteristics  
92 of the molecules involved at the interface. The basic components of the system under  
93 investigation are three: the triglyceride with three monounsaturated oleic acid residues

This is the author's peer reviewed, accepted manuscript. However, the online version of record will be different from this version once it has been copyedited and typeset.

PLEASE CITE THIS ARTICLE AS DOI: 10.1063/1.50079883

94 which stands for the oil phase, the protein Apovitellenin I coming from the egg yolk LDL  
95 and, finally, water. In this Section a general description of the macroscopic system to be  
96 modeled is provided, together with the adopted simplifications.

97 An example of a food emulsion where the egg yolk is widely used as an emulsifier is  
98 mayonnaise. This is a stable liquid-liquid emulsion with a high content of the dispersed oil  
99 phase. In this work a regular mayonnaise with around 70% of fat content<sup>1</sup> is considered and  
100 the experimental work of Dubbelboer *et al.*<sup>3</sup> is used as a reference to identify the ingredients  
101 of the mayonnaise, especially the molecules to play a primary role at the oil/water interface.  
102 It is important to highlight that also in this work the dispersed phase consists of the soybean  
103 oil, while the chemical species that act as surfactants are derived from the egg yolk. These  
104 two components characterize the specific type of mayonnaise studied, therefore a further  
105 description of the vegetable oil and the egg yolk used in the production of the food emulsion  
106 is presented in order to correctly select the molecules to be modeled.

107 Regarding the dispersed phase, a fully refined soybean oil is employed in which the  
108 triglyceride molecules are present with a concentration larger than 99%.<sup>55</sup> Triglycerides are  
109 tri-esters consisting of a glycerol bound to three fatty acid molecules. Based on the number of  
110 double bonds and the chain length, the fatty acids occurring in triglycerides of the soybean oil  
111 are saturated, monounsaturated and polyunsaturated with 16 or 18 carbon atoms according  
112 to an internal distribution.<sup>55</sup> For the sake of simplicity, here homotriglycerides are taken  
113 into account where the three fatty acids are identical (without an internal distribution). In  
114 particular, the triglyceride molecules with three monounsaturated oleic acid residues (18  
115 carbon atoms for chain) will be modeled as the representative of the oil phase, instead of  
116 hydrocarbons as it was done in previous DPD works on similar emulsions.<sup>52-54</sup> It should be  
117 noted that the protein adsorption to different hydrophobic materials may cause differences  
118 in the conformation of the adsorbed molecule; in this sense our simplification may have  
119 an impact that it is difficult to quantify. That being said, it is known that the modeling  
120 of a simpler hydrocarbon–water system instead of a triglyceride–water system might not  
121 necessarily lead to realistic results,<sup>56</sup> therefore a triglyceride–water system was modeled in  
122 this work.

123 The second fundamental component in the mayonnaise production is the hen egg yolk.  
124 It is mainly composed of two fractions – plasma and granules – which are natural nano-  
125 and micro-assemblies. Plasma contains a large quantity of lipids structured as low-density

This is the author's peer reviewed, accepted manuscript. However, the online version of record will be different from this version once it has been copyedited and typeset.

PLEASE CITE THIS ARTICLE AS DOI: 10.1063/1.50079883

lipoproteins (LDLs), whereas granules are mainly composed of proteins aggregated in micrometric assemblies.<sup>7</sup> Assuming a pH equal to 3.8 for the mayonnaise,<sup>57</sup> plasma proteins represent about 2/3 of oil-water interface in acidic conditions (at all ionic strengths).<sup>7</sup> Previous works have shown that LDLs are likely to play primary roles in the formation and stabilization of egg yolk-based emulsions.<sup>7,58-61</sup> Consequentially, LDLs are considered to contribute mainly to yolk emulsifying properties.<sup>7</sup> LDLs are spherical nanoparticles (17-60 nm) with a lipid core of triglycerides and cholesterol esters in a liquid state surrounded by a monofilm of phospholipids and apoproteins.<sup>7,62-67</sup> The LDL adsorption mechanism at the oil-water interface was investigated by several works.<sup>7,67-71</sup> In fact, LDLs serve as vectors of surfactant constituents (proteins and phospholipids) that could not be soluble in water until they reach the interface. The adsorption of apoproteins and phospholipids at the interface lead to the formation of a film that stabilize the emulsion.<sup>69</sup> Therefore, both apoproteins and phospholipids are essential to understand the interfacial properties of egg yolk LDLs. The protein identified as Apovitellenin I is considered to be the most surface-active, among the apoproteins contained in LDL.<sup>64,67</sup> Due to its structure and composition, which combines amphipathic character and flexibility, Apovitellenin I shows a great capacity to adsorb at the oil-water interface in emulsions.<sup>67</sup> In LDL, Apovitellenin I is mostly present as a homodimer, thus containing two identical polypeptide chains of 82 amino acid residues which are linked by a single disulfide bond at the cysteine residue.<sup>64,67</sup> The sequence of the mature protein is available in the UniProtKB database<sup>72</sup> under the accession number P02659 ([www.uniprot.org/uniprot/P02659](http://www.uniprot.org/uniprot/P02659)). However, the detailed 3D structure and other physico-chemical information of Apovitellenin I are not available in the literature to the best of authors' knowledge, increasing the complexity of its modeling approach. The presence of salts, small surfactant molecules (phospholipids) or other additives is here neglected since only the emulsifying capacity of the considered egg yolk LDL protein is investigated. Furthermore, the pH of the system is kept constant and equal to 3.8. The molecular model of the oil-water interface is then described in the following sections.

### III. THEORETICAL BACKGROUND

In this Section only the main basic concepts of the standard Dissipative Particle Dynamics (DPD) method are presented, while a further detailed description of both MD and DPD

This is the author's peer reviewed, accepted manuscript. However, the online version of record will be different from this version once it has been copyedited and typeset.

PLEASE CITE THIS ARTICLE AS DOI: 10.1063/1.50079883

156 techniques can be found in the literature<sup>25,27-29,73,74</sup> and in the Supplementary Material.

157 DPD is a stochastic mesoscale particle model that it has been devised to allow the sim-  
 158 ulation of the dynamics of mesoscopic particles. Unlike classic Molecular Dynamics, each  
 159 DPD particle  $i$ , called bead, represents a molecular cluster (a molecule fragment or a group  
 160 of solvent molecules) rather than an individual atom. The major difference between MD  
 161 and DPD, apart from the coarse-grained nature of the molecules, is the nature of the forces  
 162 between them. The force acting on each bead  $i$  contains three parts: the conservative,  
 163 dissipative, and stochastic (random) forces, each of which is pairwise additive. Here the  
 164 conservative force felt by bead  $i$  includes: 1) contributions from repulsive interactions with  
 165 surrounding beads; 2) contributions due to the springs connecting bead  $i$  to other beads in  
 166 the same molecule; and 3) contributions due to angle bending interactions. The repulsive  
 167 force  $\mathbf{F}_{ij}^r$ , which is modeled as a soft repulsion between beads  $i$  and  $j$ , is defined as follows:

$$\mathbf{F}_{ij}^r = \begin{cases} a_{ij}(1 - r_{ij}/r_c)\hat{\mathbf{r}}_{ij} & \text{if } r_{ij} \leq r_c \\ 0 & \text{if } r_{ij} > r_c \end{cases}, \quad (1)$$

168 where  $r_{ij} = |\mathbf{r}_i - \mathbf{r}_j|$  is the distance between beads  $i$  and  $j$  at positions  $\mathbf{r}_i$  and  $\mathbf{r}_j$  respectively,  
 169 and  $\hat{\mathbf{r}}_{ij} = (\mathbf{r}_i - \mathbf{r}_j)/r_{ij}$  is the direction between the two beads. The parameters  $a_{ij}$  are  
 170 the DPD interaction parameters defined for each bead pair, while  $r_c$  stands for the cutoff  
 171 distance. For the system investigated in this work, their definition will be given in the  
 172 Section IV B and they will be here used as fitting parameters for the calibration of the DPD  
 173 model. The adjacent beads are constrained with permanent lengths and angular bonds. In  
 174 this study, the bonds were modeled using harmonic spring quadratic potentials given as:

$$U_{ij}^S = k_S(r_{ij} - l_H)^2, \quad (2)$$

$$U_{ijk}^A = k_A(\theta_{ijk} - \theta_H)^2, \quad (3)$$

176 where  $l_H$  and  $\theta_H$  are the equilibrium lengths and angles for beads  $i$ ,  $j$  and  $k$ . The stiffness  
 177 of the length and angular bond constraints is defined by the values of  $k_S$  and  $k_A$ .

178 As it is customary in DPD, the quantities here reported have to be considered reduced  
 179 (dimensionless) and the scaling factors for the main properties (mass, length, time, energy)  
 180 will be explained in Section IV C. Finally, it is important to point out that the coarse-  
 181 graining of the molecular structures and the soft interactions allow larger systems to be  
 182 modeled over significantly longer times than with (atomistic scale) molecular modeling,<sup>41,74</sup>

This is the author's peer reviewed, accepted manuscript. However, the online version of record will be different from this version once it has been copyedited and typeset.

PLEASE CITE THIS ARTICLE AS DOI: 10.1063/1.50079883

183 thus allowing the dynamics of mesoscopic systems to be followed over relevant time scales  
184 as well as length scales.

#### 185 IV. MODELING DETAILS

186 In order to consider both the complex composition of the emulsion and the equilibration  
187 time required by macro-molecules to re-arrange at interfaces, the DPD approach is employed  
188 in which the parameter calibration is based on MD simulations. Next sections will present  
189 the setup of MD simulations, the DPD model development in which both the coarse-graining  
190 procedure and the calibration of parameters are explained and, finally, definitions of the main  
191 physical properties investigated here.

##### 192 A. MD simulations

193 The purpose of all-atom MD simulations is to use their results to calibrate the DPD  
194 parameter set. Only MD simulations of one protein molecule in bulk phases (water or oil)  
195 were performed rather than the entire ternary interfacial system due to the size of the latter  
196 which would require excessive computational time. An initial guess of both protein and  
197 triglyceride structures was manually made from scratch via a molecule editor. In particular,  
198 Figure 2a shows the all-atom protein model. It can be clearly seen the disulfide bond linking  
199 two identical polypeptide chains. Furthermore, the N- and C- terminal amino acid residues  
200 and, if applicable, the functional group of side chains were protonated or deprotonated by  
201 comparing their corresponding  $pK_a$  with the pH of the solution.<sup>75</sup> Thus, at pH 3.8 the  
202 net charge of the protein homodimer results equal to 16  $e$  and the protein molecular mass  
203  $M$  is 18675.6 Da. MD simulations were performed using the OPLS-AA force field,<sup>76,77</sup>  
204 while water was described by the TIP3P water model.<sup>78</sup> A cutoff of 7.5 Å was used for  
205 long-range interactions, and both electrostatic and van der Waals interactions were handled  
206 using a smooth particle mesh Ewald summation method (SPME).<sup>79</sup> For the protein and  
207 the triglyceride, first 20-ps simulation in vacuum with a time step of 1 fs was performed  
208 on the single molecule to relax its initial structure. Before solvation with water or oil,  
209 the protein was centered in a rectangular box with a minimum distance of any part of  
210 the molecule defined to be at least 1 nm from box walls in order to satisfy the minimum



This is the author's peer reviewed, accepted manuscript. However, the online version of record will be different from this version once it has been copyedited and typeset.

PLEASE CITE THIS ARTICLE AS DOI: 10.1063/1.50079883

211 image convention when using periodic boundary conditions. According to the reproduced  
212 environment, the box was filled with respectively 15994 water or 325 triglyceride molecules,  
213 plus 16  $\text{Cl}^-$  counterions to ensure the electroneutrality of the system. Thus, the resulting  
214 MD box contains a total of 50694 or 56987 atoms in the case of protein in water or oil bulk  
215 respectively. After a simple energy minimization to ensure that the system had no steric  
216 clashes or inappropriate geometry, a 0.5-ns NPT (i.e., constant number of particles, pressure,  
217 and temperature) equilibration simulation at ambient pressure (1 atm) and temperature (298  
218 K) was performed. Pressure and temperature were fixed using the Berendsen barostat and  
219 thermostat<sup>80</sup> and the Verlet algorithm was used to integrate the equations of motion with an  
220 increased time step of 2 fs. To verify that the system was at the equilibrium, the fluctuations  
221 in the temperature, pressure, density, and potential energy were monitored. In particular,  
222 the average density reached during the last 0.2 ns of equilibration simulation was equal  
223 to 1059.57 and 921.85  $\text{kg}/\text{m}^3$  respectively for the protein in water and in oil system, both  
224 with fluctuations in the 0.1%. Finally, NVT (i.e., constant number of particles, volume,  
225 and temperature) production simulations ranging from 2 to 6 ns were performed to collect  
226 statistically averaged results by saving particle trajectories every 250 time steps.

## 227 B. Coarse-graining procedure and parameter calibration

228 The main steps of the DPD model development are summarized in a schematic diagram  
229 in Figure 1, in which each stage is explained in this Section.

231 The first step toward a realistic DPD molecular model is to obtain the coarse-grained (CG)  
232 representation of the molecules together with their full parameter set of both inter- and intra-  
233 molecular interactions. For this scope, the Automated Fragmentation and Parametrization  
234 (AFP) method is used and here a very brief introduction to this approach is provided. For  
235 a fully detailed discussion on it, the reader can refer to the work of Fraaije *et al.*<sup>81</sup>.

236 Starting from their fully atomistic representations, the molecules involved in the investi-  
237 gated system are fragmented according to a scoring function, through a simulated annealing  
238 function that cuts through bonds; the optimal bond fission pattern is preserved and the  
239 fragments are stored. The scoring function is here defined as:

$$S = \left(1 - \frac{V}{V_0}\right)^2, \quad (4)$$

This is the author's peer reviewed, accepted manuscript. However, the online version of record will be different from this version once it has been copyedited and typeset.

PLEASE CITE THIS ARTICLE AS DOI: 10.1063/1.50079883

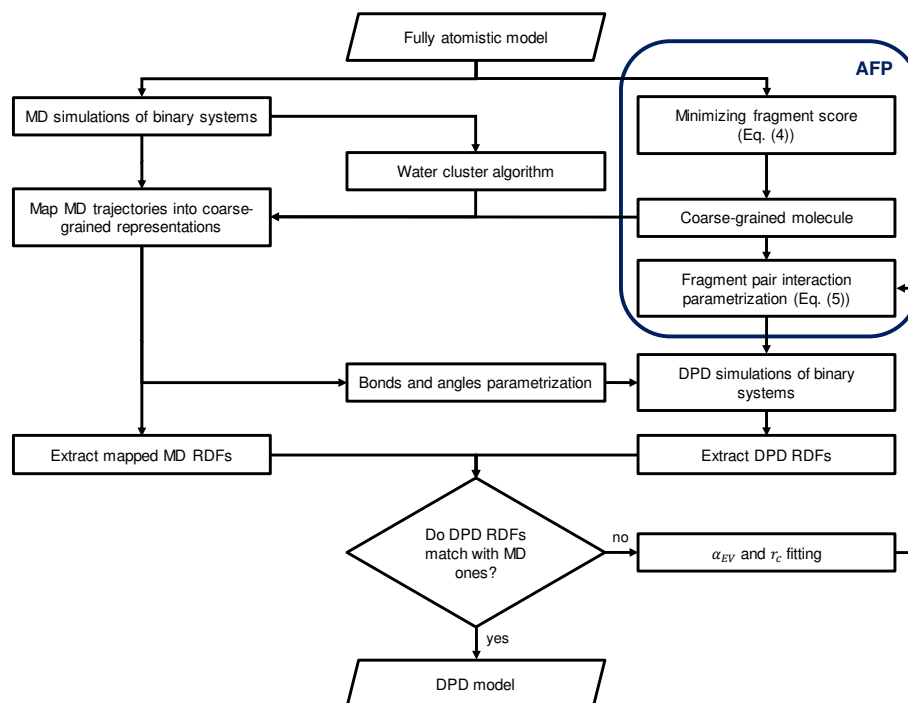


FIG. 1. Schematic diagram of the main stages followed in this work to develop the DPD model. See Section IV B for details of each step.

240 where  $V$  is the volume of the fragment and  $V_0$  is the reference volume of a cluster of three  
 241 water molecules in its lowest energy conformation (i.e., the reference volume used here is  
 242 equal to  $67.7 \text{ \AA}^3$  as in the original AFP work<sup>81</sup>). In this approach the molecule-unique frag-  
 243 mentation is used in order to preserve as much as possible of the properties of the molecule.  
 244 This means that the fragments are not database-unique, as is customary in coarse-grained  
 245 simulations, but completely specific to a given molecule. By applying this fragmentation  
 246 technique, the triglyceride molecule and the homodimer Apovitellenin I are comprised of  
 247 20 and 500 beads respectively, while each water bead corresponds to three atomistic water  
 248 molecules. In particular, Figure 2 shows the all-atom (a) and the corresponding coarse-  
 249 grained (b) representation of the protein molecule.

251 In the AFP framework, the interaction DPD parameter  $a_{ij}$  is split into two contributions,

This is the author's peer reviewed, accepted manuscript. However, the online version of record will be different from this version once it has been copyedited and typeset.

PLEASE CITE THIS ARTICLE AS DOI: 10.1063/1.50079883

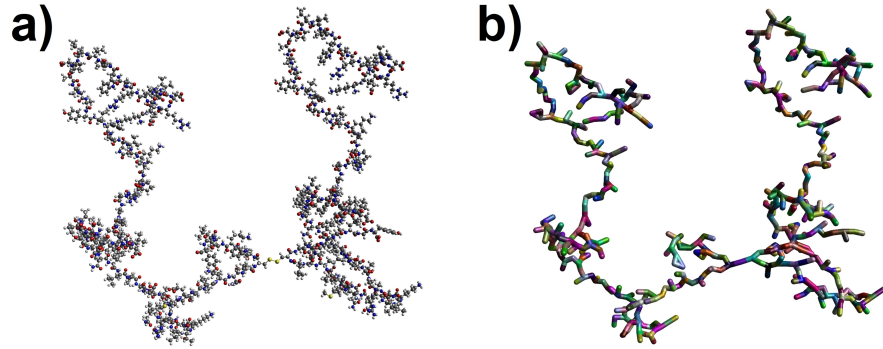


FIG. 2. All-atom (a) and corresponding coarse-grained (b) model obtained via AFP of Apovitelenin I. DPD beads are represented by colored fragments, highlighting the bond fission pattern.

one from the excluded volume and the second from the residual interactions:

$$a_{ij} = \alpha_{EV}v_i v_j + \alpha_{res}\sqrt{v_i v_j}\beta\Delta G_{res,ij}, \quad (5)$$

where  $v_i = V_i/V_0$  is the scaled molecular volume of fragment  $i$ ,  $\beta = 1/k_bT$ ,  $\alpha_{EV}$  and  $\alpha_{res}$  represent two global adjustable parameters and  $\Delta G_{res,ij}$  is the residual Gibbs energy of mixing of a *hypothetical* equimolar mixture of fragments  $i$  and  $j$ . The Gibbs energy of mixing was calculated through COSMO-RS calculations,<sup>82,83</sup> using the charge envelope of the fragments (the so-called sigma profiles). The COSMO charge envelope is here computed via a modified version of AM1,<sup>84-86</sup> using atomic partial charges derived from the charge equilibration (QEq) method.<sup>87</sup> By definition the residual Gibbs energy of mixing between identical fragments is zero, i.e.,  $\Delta G_{res,ii} = 0$ , thus it follows trivially that  $a_{ii}$  is reduced only to the excluded volume contribution and, in particular, for water bead self-interaction  $a_{ww} = \alpha_{EV}$ . It is also important to point out here that the bead-size effect is taken into account in the definition of DPD  $a_{ij}$  parameter given in Eq. (5) by considering the fragment volume scaled with respect to the reference volume,  $V_0$ , of a cluster of three water molecules. This allows to consider a constant DPD base unit of length,  $h$ , for all fragments irrespective of size or composition. As in the original AFP work,<sup>81</sup> here the value of  $h$  is assumed equal to 7.65 Å as the yardstick for length in DPD approach. This value corresponds to five 3-mer water clusters per cell of size  $h^3$ , or, in terms of the DPD dimensionless unit system, this corresponds to a density of 5 for water under ambient conditions. The soft-core repulsion

This is the author's peer reviewed, accepted manuscript. However, the online version of record will be different from this version once it has been copyedited and typeset.

PLEASE CITE THIS ARTICLE AS DOI: 10.1063/1.50079883

270 potential employed here is devoid of the short-range Lennard-Jones divergence. Also, the  
271 typical long-range electrostatic Coulomb term is avoided completely, through using the close-  
272 contact electrostatic interaction of the COSMO model. Both interactions are therefore  
273 replaced by a soft repulsive potential that is local, with a length scale limited to the cutoff,  
274  $r_c$ . Hence, in AFP approach the fragment-specific chemical information is condensed in only  
275 one parameter: the DPD  $a$  parameter. The magnitude of the repulsion (not the spatial  
276 extension) is modified depending on the volume of the underlying molecular fragment, and  
277 residual interactions. In order to map the characteristics of the atomistic models into the  
278 DPD system, MD simulations of protein in water and oil bulks were used to extract molecular  
279 characteristics such as radial distribution functions as well as the distributions of lengths  
280 and angles for molecules bonded with length and angular bonds. To make MD and DPD  
281 models physically comparable, it is necessary to map atomistically detailed trajectories into  
282 their corresponding coarse-grained representations considering a length scale factor,  $h$ , to  
283 convert atomistic coordinates and MD box dimensions into a CG model. When dealing with  
284 the triglyceride and the protein in which their fragmentation information has been already  
285 well-defined through the AFP approach, the mapped MD trajectories of such molecules  
286 are easily determined by replacing the fully atomistic coordinates with the centre-of-mass  
287 positions of provided molecular fragments. However, in the case of atomistic water models,  
288 where the water particles move independently, their CG representation has to be dynamically  
289 identified. Therefore, a clustering method is required to enable the mapping of multiple  
290 water molecules into a single CG bead. Here, the water molecules clustering algorithm  
291 proposed by Pieczywek, Płaziński, and Zdunek<sup>88</sup> was employed, which is based on a step-  
292 wise iterative nearest neighbour search algorithm. The number of water molecules per bead  
293 in all clusters is kept constant and equal to the degree of coarse-graining employed here,  
294 i.e., a 3 to 1 CG ratio, corresponding to the number of clustering steps performed for each  
295 simulation time frame. This represents the major advantage compared to other approach  
296 where, instead, the total number of beads in the system have to be provided,<sup>89</sup> leading to  
297 some issues converging with the desired number of equally sized clusters. Very briefly, as the  
298 algorithm initialization, a grid of fixed-size cubes was superimposed onto the MD simulation  
299 box and initial positions of bead centers were generated by randomly choosing coordinates  
300 of water molecules from the first time frame. For each step of the algorithm, an iterative  
301 search for the unique nearest water molecule was carried out in the area adjacent to the unit

This is the author's peer reviewed, accepted manuscript. However, the online version of record will be different from this version once it has been copyedited and typeset.

PLEASE CITE THIS ARTICLE AS DOI: 10.1063/1.50079883

302 cell in which the coarse-grained bead is located. The unique nearest water molecule was  
303 defined by means of the Euclidean distance from the center-of-mass of a CG bead. When  
304 all of the CG beads had the same number of molecules assigned to them (equal to the CG  
305 ratio), the algorithm finished and the positions of the beads were updated by calculating  
306 the center-of-mass of the molecular clusters. Hence, for each MD simulation time frame, the  
307 water molecules were divided into equally sized groups based on their proximity.

308 The mapped MD trajectories were used to extract radial distribution functions (RDFs)  
309 of coarse-grained molecules. Thus, using the AFP method as a basis, a further DPD param-  
310 eter calibration was carried out by using the MD RDFs as reference curves to be compared  
311 with those extracted from DPD simulations. Since the RDF is solely determined by the  
312 conservative force,<sup>90</sup> the repulsion force coefficients was adjusted to match MD and DPD  
313 RDFs. As the specific fragment pair interactions were defined in Eq. (5), the global ad-  
314 justable parameters which serve to define the mutual repulsive interaction between *all* the  
315 beads belonging to a single type of molecule can be used to calibrate the DPD model. In  
316 particular,  $\alpha_{EV}$  and the cutoff distance,  $r_c$ , were used as fitting parameters, while for all the  
317 fragment pairs the DPD-sigma parameter was set to the standard value of  $3.0^{29}$  and  $\alpha_{res}$   
318 was kept equal to 6.1 as in the original AFP work.<sup>81</sup> Therefore, from both MD and DPD  
319 simulations of protein in water and in oil bulk, only RDFs referring to all beads belonging  
320 to water, oil, and protein were extracted and the results of the calibration are presented and  
321 discussed in Section V. Obviously, from simulations of the binary systems only water-water,  
322 oil-oil, water-protein, and oil-protein interactions can be exactly calibrated. However, the  
323 remaining interactions, i.e., oil-water and protein-protein, must be determined to build the  
324 DPD model of the ternary system. In particular, the oil-water  $\alpha_{EV}$  value was obtained by  
325 simply fitting the experimental interfacial tension between purified soybean oil and water,<sup>51</sup>  
326 found to be equal to 31-32 mN/m and independent on the presence of salt.<sup>91</sup> For the protein-  
327 protein repulsive interaction, the same  $\alpha_{EV}$  value of water-protein was arbitrarily chosen as  
328 a first guess. This value could be of paramount importance since the self-protein interaction  
329 may effect the structural configuration of the protein as well as equilibrium and dynamics  
330 properties of the ternary system. The study of protein-protein interactions needs therefore  
331 a deeper insight, which could be the scope of future works.

332 The parametrization of intra-molecular interactions (bonds and angles) of CG molecules  
333 was also based on MD simulations. The basic concept is to construct the distribution

This is the author's peer reviewed, accepted manuscript. However, the online version of record will be different from this version once it has been copyedited and typeset.

PLEASE CITE THIS ARTICLE AS DOI: 10.1063/1.50079883

334 function of each of these quantities from atomistic model simulations. By using again the  
335 molecular fragment information obtained via AFP within the atomistic MD trajectories,  
336 the distribution functions of bond lengths and bending angles were calculated based on the  
337 center of the coarse-grained fragments. Then, a robust and fast approach when dealing  
338 with hundreds of bond and angle interaction types generated from the automated coarse-  
339 graining procedure employed in this work (AFP) is to derive parameters from distributions  
340 directly,<sup>43,92,93</sup> instead of fitting each bond-stretching and bending angle potential obtained  
341 from Boltzmann inversion with a harmonic approximation.<sup>94</sup> When assuming a harmonic  
342 bond potential (Eq. (2)), the resulting distribution is a Gaussian that can be equated with  
343 the distribution of the bonds. It follows that the equilibrium bond length,  $l_H$ , is simply  
344 the average of the distribution and the bond constant,  $k_S$ , can be expressed in terms of the  
345 standard deviation of that distribution.<sup>43,92,93</sup> For angles, the same would hold for harmonic  
346 potentials (Eq. (3)), except that the angle is bounded between  $0^\circ$  and  $180^\circ$ . This means  
347 that the distribution for a purely harmonic potential will not be a Gaussian, but rather a  
348 Gaussian that is cut off at  $180^\circ$ . However, a reasonable procedure is to simply take the angle  
349 where the distribution is maximal and treating that as if it were the average, equating it to  
350 the equilibrium angle,  $\theta_H$ . Taking the standard deviation to calculate the angle potential  
351 strength,  $k_A$ , also is reasonable.<sup>43</sup> It is important to point out that this procedure is not able  
352 to capture multiple maxima and/or minima in bond and angle distributions from atomistic  
353 MD simulations.<sup>43</sup> Without a further modification, bonded interaction parameters directly  
354 derived from MD distributions can be used in DPD simulations by using a shorter time step  
355 than that typically used in DPD works (i.e.,  $\Delta t = \mathcal{O}(0.01)^{29}$ ). In fact, the exact replication  
356 of the MD structures required the strength of bonds to become too large for relatively long  
357 time step, resulting in unstable simulations.<sup>41</sup> Therefore, in order to preserve the distance  
358 and angular bond characteristics, a dimensionless time step of  $\Delta t = 0.001$  was used to  
359 integrate the DPD equations of motion.<sup>88</sup>

### 360 C. DPD simulation parameters

361 To avoid using excessively large or small numbers and to simplify the calculations, DPD  
362 systems were usually scaled by arbitrarily chosen base units. As it was already discussed  
363 in the previous subsection, the conversion factor  $h = 7.65 \text{ \AA}$  was here employed as base

364 unit of length. The mass of one water bead consisting of three water molecules equal to  
 365  $8.974 \times 10^{-26}$  kg, was used as the base mass unit. Both MD and DPD simulations were  
 366 performed at ambient temperature (298 K), giving  $k_b T = 4.11 \times 10^{-21}$  J used as the base  
 367 unit for energy, where  $k_b$  is the Boltzmann constant. The base time unit  $\tau$  was estimated by  
 368 evaluating the diffusion coefficient. This is computed from both MD and DPD simulations  
 369 by using the standard mean-squared displacement (MSD) method through the well-known  
 370 Einstein relation.<sup>25</sup> By defining the scaling factor  $S = D_{W,Exp}/D_{W,DPD} = 7.63 \times 10^{-9}$  m<sup>2</sup>/s,  
 371 where  $D_{W,Exp}$  and  $D_{W,DPD}$  are respectively the experimental water self-diffusion coefficient  
 372 at ambient conditions and the simulated one via DPD, the base unit used to convert the  
 373 reduced DPD time into real unit reads as follows:

$$\tau = \frac{h^2}{S} \approx 77 \text{ ps.} \quad (6)$$

Therefore, the real protein diffusion coefficient computed from DPD simulations was simply determined by multiplying the simulated value for the scaling factor,  $S$ .<sup>95</sup> Since no experimental measurement is available in the literature, the protein diffusion  $D$  computed via MD and DPD were compared with three correlations proposed for the prediction of protein diffusion coefficients in free solution, based on the molecular weight  $M$  (Eq. (7a)<sup>96</sup>), on the radius of gyration  $R_g$  (Eq. (7b)<sup>97</sup>), and on both the molecular weight and the radius of gyration of the protein (Eq. (7c)<sup>98</sup>), respectively:

$$D = 8.34 \times 10^{-8} \left( \frac{T}{\eta M^{1/3}} \right), \quad (7a)$$

$$D = 5.78 \times 10^{-8} \left( \frac{T}{\eta R_g} \right), \quad (7b)$$

$$D = 6.85 \times 10^{-8} \left( \frac{T}{\eta \sqrt{M^{1/3} R_g}} \right), \quad (7c)$$

374 where  $\eta$  is the solvent viscosity, i.e., 0.894 and 50 cP at 25 °C for water<sup>99</sup> and for soybean  
 375 oil,<sup>100</sup> respectively.

376 Several DPD simulation configurations were investigated in this work. In order to match  
 377 the coarse-grained characteristics from MD simulations, the binary systems were reproduced  
 378 using DPD. The MD box was scaled according to the length conversion factor  $h$  and one  
 379 CG protein molecule was located at its center. According to the binary environment, the  
 380 box was then filled with water beads or oil CG molecules to obtain the overall DPD density  
 381  $\rho = 5$ . The DPD simulations were performed with an equilibration period of  $10^5$  steps, then

This is the author's peer reviewed, accepted manuscript. However, the online version of record will be different from this version once it has been copyedited and typeset.

PLEASE CITE THIS ARTICLE AS DOI: 10.1063/1.50079883

382 followed by a production phase of  $10^6$  steps, saving particle trajectories every 250 steps.  
 383 Once DPD parameters have been calibrated as explained in the previous subsection, two  
 384 DPD configurations of the interfacial system were carried out in order to study the equilib-  
 385 rium properties at increasing protein interface concentration  $c_i$  and the protein adsorption  
 386 at the oil/water interface. Both initial configurations consisted of a central water phase  
 387 segregated by two oil phases, thus forming two planar interfaces in equidistant  $yz$ -planes.  
 388 The 50/50 oil-to-water bead ratio was kept constant for all DPD simulations and both the  
 389 number of water beads and oil CG molecules was adjusted to keep the same overall DPD  
 390 density of 5 when the protein molecules were also added in the DPD box. The equilib-  
 391 rium simulations were conducted with increasing protein interface concentration  $c_i$ , which is  
 392 simply calculated by multiplying the number of the protein molecules at each interface for  
 393 the protein molecular mass  $M$ , divided for the constant interface  $yz$ -area expressed in real  
 394 units. The protein molecules were initially located at the oil-water interface to make sure  
 395 that both interfaces contain the same number at equilibrium in order to perform averages  
 396 on both interfaces. For equilibrium DPD simulations, the box was an orthorhombic cell of  
 397 reduced size  $L_x \times L_y \times L_z$ , where  $L_y = L_z = 32$  and  $L_x$  was properly adjusted up to 52 based  
 398 on the protein molecule number to allow both interfaces to be independent. Simulations  
 399 were run for  $2.5 \times 10^5$  equilibration steps and for a production period of  $10^6$  steps, saving  
 400 time frame data for post-processing every 500 steps. Here the interfacial tension,  $\sigma_{\text{DPD}}$ ,  
 401 was computed by integrating the difference between normal and tangential stress across the  
 402 interface separating the segregated components.<sup>101</sup> Thus, if the normal to the interface lies  
 403 along the  $x$ -direction, the interfacial tension is deduced from the local components of the  
 404 pressure tensor:

$$\sigma_{\text{DPD}} = \frac{1}{2} \int (p_N^* - p_T^*) dx = \frac{1}{2} \int \left( p_{xx}^* - \frac{1}{2} (p_{yy}^* + p_{zz}^*) \right) dx, \quad (8)$$

405 where  $p_N^*$  and  $p_T^*$  are the normal and tangential components of the pressure tensor profile  
 406 in reduced DPD units. The factor 1/2 before the integral sign is due to the presence of two  
 407 symmetric interfaces in the DPD simulation box when using periodic boundary conditions.  
 408 Since the oil droplets of a food emulsion have a diameter of the order of microns,<sup>3</sup> it is reason-  
 409 able to neglect the curvature effect when modeling the interfacial system at the nano-scale,  
 410 thus allowing to use the above formula, valid for planar geometry only.<sup>101</sup> The conversion of  
 411  $\sigma_{\text{DPD}}$  to real units operates as follows:  $\sigma_{\text{calc}} = \frac{k_b T}{h^2} \sigma_{\text{DPD}}$ . The quantity  $\sigma_{\text{calc}}$  can be directly



412 compared with experimentally measured interfacial tension. The free protein adsorption at  
413 the oil/water interface was also studied by locating one protein molecule in the center of  
414 an orthorhombic DPD box  $L_x \times L_y \times L_z$ , where  $L_y = L_z = 20$  and  $L_x$  was ranged from 40  
415 to 56 in order to properly increase the mutual initial distance between the protein center  
416 and the interface. In addition, the adsorption at the oil/water interface was tested for an  
417 LDL-like particle configuration by initially creating a small droplet of 15 oil CG molecules  
418 surrounded by one protein molecule. These latter DPD simulations were performed with  
419  $2 \times 10^5$  equilibration steps and a production period of up to  $4 \times 10^6$  steps, saving simulation  
420 time frames every 500 steps to check if the protein adsorption has taken place.

421 Apart from the water cluster algorithm, which was performed in the MATLAB environment,<sup>88</sup>  
422 all MD and DPD simulation setup, runs, and post-processing analyzes were conducted within  
423 the CULGI software package,<sup>102</sup> together with all other tools and algorithms employed in  
424 this work.

## 425 V. RESULTS AND DISCUSSION

426 The results of the DPD model calibration explained in Section IV B are shown in Figure  
427 3, where the distance is expressed in real units, and in Table I. Using the MD RDFs as  
428 references, the DPD RDFs were adjusted in order to best match curve heights and shapes  
429 by calibrating both  $\alpha_{EV}$  and  $r_c$  of molecule bead pairs. These two terms define both the  
430 magnitude (via Eq. (5)) and the spatial extension of the repulsive force (Eq. (1)). Typically,  
431 in standard DPD the cutoff value also represents the base unit of length and, therefore, is  
432 often set equal to 1 in dimensionless unit.<sup>29</sup> In contrast, here the dimensionless value of  $r_c$   
433 resulting from fitting the first peaks of RDF curves shown in Figure 3 was found to be equal  
434 to 0.7. Hence, the cutoff,  $r_c$ , and the length factor,  $h$ , were decoupled in order to assure  
435 both the constant DPD number density of 5 and the repulsive force calibration. The results  
436 of  $\alpha_{EV}$  fitting are summarized in Table I. Although the oil-water  $\alpha_{EV}$  turned out to be  
437 substantially smaller than all the others in Table I, the overall repulsion between water and  
438 oil beads was properly reproduced due to the two contributions in Eq. (5) and a cutoff,  $r_c$ ,  
439 equal to 1 in this specific case, in which a sophisticated calibration was not needed.

442 The molecular model is tested and the main findings are presented here, paying a particu-  
443 lar attention to verify the emulsifying behaviour of Apovitellenin I at the oil/water interface.

This is the author's peer reviewed, accepted manuscript. However, the online version of record will be different from this version once it has been copyedited and typeset.

PLEASE CITE THIS ARTICLE AS DOI: 10.1063/1.50079883

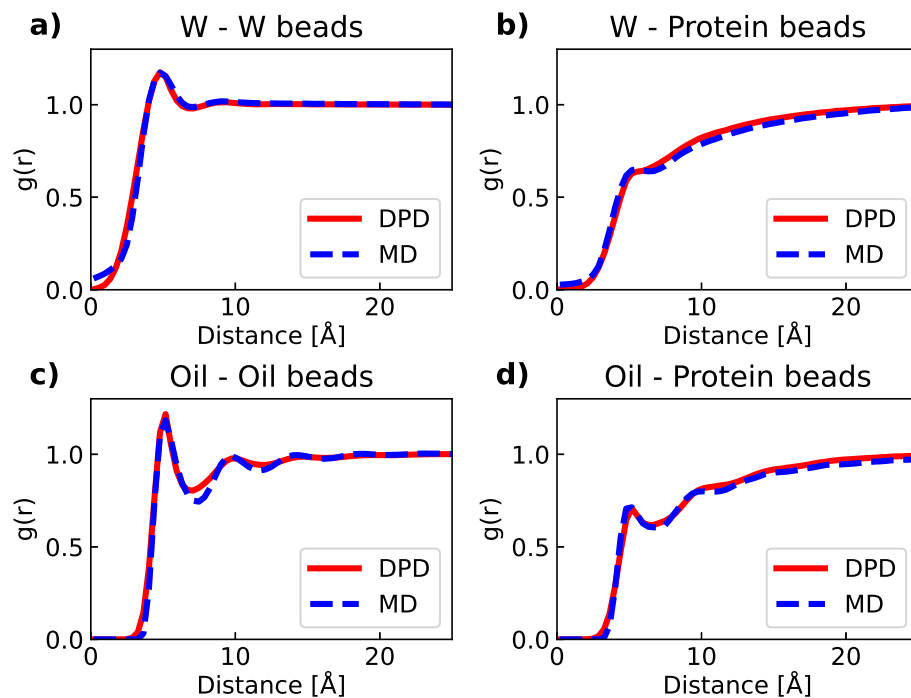


FIG. 3. Results of the DPD parameter calibration of water-water (a), water-protein (b), oil-oil (c), and oil-protein (d) interactions based on matching RDFs of the mapped MD reference model (dashed blue line) with corresponding RDFs extracted from DPD simulations (solid red line).

444 First, preliminary structural and dynamic quantities of the protein are estimated by per-  
 445 forming both MD and DPD simulations of one protein molecule in bulk phases. Then, the  
 446 DPD simulation results of the ternary system are discussed in terms of both equilibrium  
 447 and dynamic aspects.

448 Table II reports End-to-End distance and radius of gyration mean values and standard  
 449 deviations of Apovitellenin I in water and oil bulks computed via MD and DPD simulations.  
 450 The MD values were averaged over the simulation time, meanwhile 10 independent DPD  
 451 simulations with the same initial configuration were carried out from which the reported  
 452 values are extrapolated by computing their respective arithmetically averaged frequency  
 453 distributions. It is important to recall that Apovitellenin I is modeled here as a homodimer,

This is the author's peer reviewed, accepted manuscript. However, the online version of record will be different from this version once it has been copyedited and typeset.

PLEASE CITE THIS ARTICLE AS DOI: 10.1063/1.50079883

TABLE I. Values of the global parameter  $\alpha_{EV}$  used in Eq. (5) to define the mutual repulsion between all the beads belonging to water, oil, and protein in the DPD model of this work. The cutoff distance,  $r_c$ , is equal to 0.7 unless otherwise specified.

$\alpha_{EV}$	W	Oil beads	Protein beads
W	25 <sup>a</sup>	-	-
Oil beads	8.5 <sup>b</sup>	100	-
Protein beads	40	100	40 <sup>c</sup>

<sup>a</sup> Exactly corresponding to  $a_{ww}$ .

<sup>b</sup> Value obtained by fitting experimental interfacial tension between soybean oil and water,<sup>91</sup> with a cutoff distance,  $r_c$ , equal to 1.

<sup>c</sup> Arbitrarily chosen equal to the water-protein value.

454 so the two polypeptide chains are labeled as 1 and 2 in Table II where the End-to-End  
 455 distance is that between the N-terminal and the C-terminal of each chain, while the protein  
 456 radius of gyration refers to the homodimer itself. By looking at mean values reported in  
 457 the Table II, it can be noticed that a good accordance between the two molecular technique  
 458 is achieved. The largest differences are only related to the chain 1 End-to-End distance  
 459 and the radius of gyration of the protein in water environment. The MD radius of gyration  
 460 data suggest that the protein is more compact in water than in oil environment, while an  
 461 opposite trend is detected via DPD. Another considerable dissimilarity regards the standard  
 462 deviation values calculated with the two techniques. Both MD and DPD were able to  
 463 identify a smaller error of the respective quantity in oil than in water bulk meaning a less  
 464 flexible protein structure in the former environment than in the latter. However, all the DPD  
 465 standard deviations are significantly higher than those obtained via MD. This might be due  
 466 to two main reasons. First, combining distributions from independent DPD simulations into  
 467 a single arithmetically averaged distribution involves that the variance of the averaged one is  
 468 always at least as large as the minimum of the variances of input distributions.<sup>103</sup> Secondly,  
 469 the soft potential applied in the DPD force field can provide less steric hindrance compared  
 470 to the Lennard-Jones potential used in MD. Moreover, the higher variation in DPD than  
 471 MD may be related to the lack of additional bond constraints for intra-protein molecular  
 472 interaction<sup>46,104</sup> in the present DPD framework, thus assuming a completely flexible nature

This is the author's peer reviewed, accepted manuscript. However, the online version of record will be different from this version once it has been copyedited and typeset.

PLEASE CITE THIS ARTICLE AS DOI: 10.1063/1.50079883

TABLE II. End-to-End distance and radius of gyration mean values and standard deviations of Apovitellenin I in water and oil bulk phases computed via MD and DPD simulations.

			MD	DPD <sup>a</sup>
Apovitellenin I in Water	<b>End-to-End distance</b> [Å]	Chain 1	50.46 ± 2.93	62.06 ± 18.84
		Chain 2	69.84 ± 2.82	65.87 ± 18.37
	<b>Radius of gyration</b> [Å]		24.98 ± 0.50	35.67 ± 5.26
Apovitellenin I in Oil	<b>End-to-End distance</b> [Å]	Chain 1	57.22 ± 0.96	58.38 ± 14.59
		Chain 2	64.49 ± 0.49	63.39 ± 14.20
	<b>Radius of gyration</b> [Å]		27.04 ± 0.13	29.39 ± 2.84

<sup>a</sup> The reported values are extrapolated from respective frequency distributions arithmetically averaged over 10 independent simulations.

473 of Apovitellenin I without a specific secondary structure. This latter explanation can be  
 474 also given to the opposite trend of the mean value of the protein radius of gyration reported  
 475 by means of MD and DPD in the two bulk phases.

477 Table III shows the comparison of diffusion coefficient values,  $D$ , of Apovitellenin I in  
 478 water and oil bulk calculated by means of three correlations found in the literature (Eq.  
 479 (7)<sup>96–98</sup>) and computed from MD and DPD simulations. MD protein radius of gyration in the  
 480 respective solution reported in Table II are used in expressions based on such a property (Eqs.  
 481 (7b) and (7c)). Table III also reports the diffusion errors in terms of ranges of variability.  
 482 In particular, the accuracy of correlation results was taken from the corresponding previous  
 483 works,<sup>96–98</sup> meanwhile MD and DPD uncertainties were directly estimated from simulations.  
 484 As it can be seen, both correlation and simulation results show a difference in the protein  
 485 diffusion coefficient of at least one order of magnitude between the water and oil solution.  
 486 The larger diffusion coefficient in water than in oil is mostly likely due to the larger oil  
 487 viscosity than the water one that can be responsible of the limited mobility of Apovitellenin  
 488 I in oil phase. By comparing the results for water environment, MD and DPD give a  
 489 remarkable agreement between them although all the correlations indicate a slightly higher  
 490 value. On the other hand, the accordance on simulation results is relatively lost when  
 491 dealing with oil bulk, but the DPD value is noticeably close to those predicted via empirical

TABLE III. Comparison of diffusion coefficient values of Apovitellenin I in water and oil bulk as predicted by three correlations (Eq. (7)) and as computed from MD and DPD simulations.

$D \times 10^{-12}$ [m <sup>2</sup> /s]	Correlation results			MD	DPD <sup>a</sup>
	Eq. (7a) <sup>96</sup>	Eq. (7b) <sup>97</sup>	Eq. (7c) <sup>98</sup>		
Apovitellenin I in Water	82.3 – 127.2	65.7 – 89.0	80.6 – 97.0	22.7 – 24.0	20.9 – 26.1
Apovitellenin I in Oil	1.47 – 2.27	1.10 – 1.45	1.40 – 1.65	0.296 – 0.297	1.97 – 2.92

<sup>a</sup> Averaged on 10 independent simulations.

492 correlations. It is also important to highlight here that the diffusion coefficient of proteins  
 493 in solution computed by molecular simulation techniques tends to be underestimated when  
 494 compared to the true value.<sup>105</sup> That being said, although it is really hard to validate the  
 495 data reported in Tables II and III without experimental evidence, it is possible to affirm  
 496 that molecular modeling techniques lead to very reasonable results.

498 Let us move now on the discussion of the ternary system made by oil, water and pro-  
 499 tein via DPD simulations. In order to study the equilibrium properties of such a system,  
 500 the starting configuration of the DPD box consists of two symmetrical interfaces due to  
 501 the periodic boundary conditions applied in the three directions. Figure 4 shows the equi-  
 502 librated DPD boxes representing the oil-water interface where Apovitellenin I acts as the  
 503 surfactant at increasing protein surface concentrations and by highlighting the planar inter-  
 504 faces. Figure 5 reports profiles of the number density of oil, water and protein (i) and stress  
 505 profiles (difference between normal and tangential pressures,  $p_N^* - p_T^*$ ) (ii) along the nor-  
 506 malized  $x$ -direction normal to the interfaces at increasing protein interface concentrations  
 507 corresponding to those of Figure 4 (a, b, and c). The dashed lines represent the interface  
 508 position in the initial DPD configuration. It points out the initial phase separation and  
 509 the resulting mutual interpenetration of each component at equilibrium. The profile plots  
 510 show the symmetry of the equilibrated ternary system and define the interfacial region that  
 511 contains the protein layer and the bulk region that lies between the interfaces. As it can be  
 512 seen in Figures 5 a.i), b.i) and c.i), the most interesting result is that the protein molecules  
 513 penetrate the water bulk to a much larger extent than the oil bulk, especially at higher  
 514 interface protein concentrations. As expected by looking at Table I, this is mostly likely due  
 515 to the higher overall repulsion between protein and oil than that between protein and wa-

This is the author's peer reviewed, accepted manuscript. However, the online version of record will be different from this version once it has been copyedited and typeset.

PLEASE CITE THIS ARTICLE AS DOI: 10.1063/1.50079883

516 ter. By looking at Figures 5 a.ii), b.ii) and c.ii), the mechanical equilibrium of the system is  
517 reached in both oil and water phases since the stress profiles fluctuate with small oscillations  
518 around zero in the bulk regions. As a consequence, the local contribution to the interfacial  
519 tension is located only at the interfaces, with an increase in the stress in the protein region.  
520 Therefore, the accuracy of the interfacial tension calculation is achieved. In order to avoid  
521 size effects along  $x$ -axis and allow both interfaces to be independent, the bulk phases must  
522 be large enough to reach the mechanical equilibrium by increasing the  $L_x$  dimension as the  
523 number of protein molecules increases keeping the interface  $yz$ -area constant.

525 Figure 6 reports the trend of the protein layer thickness (a), the protein mean radius of  
526 gyration,  $\langle R_{g,Protein} \rangle$  (b), and, finally, the interfacial tension (c) as a function of the interface  
527 concentration of Apovitellenin I. Three independent DPD runs were carried out and the av-  
528 eraged values are shown together with the corresponding standard deviations. Error bars are  
529 generally smaller than symbols indicating a high reproducibility of the current DPD model.  
530 The most remarkable result is the interfacial tension decrease as the protein interface con-  
531 centration increases. This trend clearly evidences the capability of Apovitellenin I to behave  
532 as a surfactant. As expected, the minimum value of the interfacial tension is reached at the  
533 saturation of the interface, which does no longer allow direct interactions between oil and  
534 water. As shown in Figure 6c, the saturation is obtained at the protein interface concentra-  
535 tion equal to 3.0-3.5 mg/m<sup>2</sup>, where the interfacial tension ranges between 8 and 10 mN/m.  
536 The maximum protein coverage (about 3.0 mg/m<sup>2</sup>) of the present system is in line with  
537 that observed in an experimental work where the oil-in-water emulsion stabilized by flexible  
538 proteins (caseins) was studied.<sup>106</sup> Moreover, Dauphas *et al.*<sup>69</sup> reported that the equilibrium  
539 interfacial tension for the oil-water interface with adsorbed LDL film at pH 3 is 9.5 mN/m,  
540 which is markedly consistent with our result. It is also important to highlight that, when  
541 no protein molecules are added, the interfacial tension between water and oil phase mod-  
542 eled as homotriglycerides is accurately reproduced in agree with the experimental value.<sup>1,91</sup>  
543  $\langle R_{g,Protein} \rangle$  (Figure 6b) is computed from the mean value of the protein  $R_g$  distribution, fur-  
544 ther averaged over 3 DPD simulations. Therefore,  $\langle R_{g,Protein} \rangle$  provides information about  
545 the conformation and packing of protein molecules at the interface. At low concentration,  
546 the protein radius of gyration is higher than its corresponding DPD value in both bulk situ-  
547 ations (see Table II). This can indicate that, when very few protein molecules are absorbed  
548 at the oil-water interface, they assume a more elongated conformation than that in water or

This is the author's peer reviewed, accepted manuscript. However, the online version of record will be different from this version once it has been copyedited and typeset.

PLEASE CITE THIS ARTICLE AS DOI: 10.1063/1.50079883

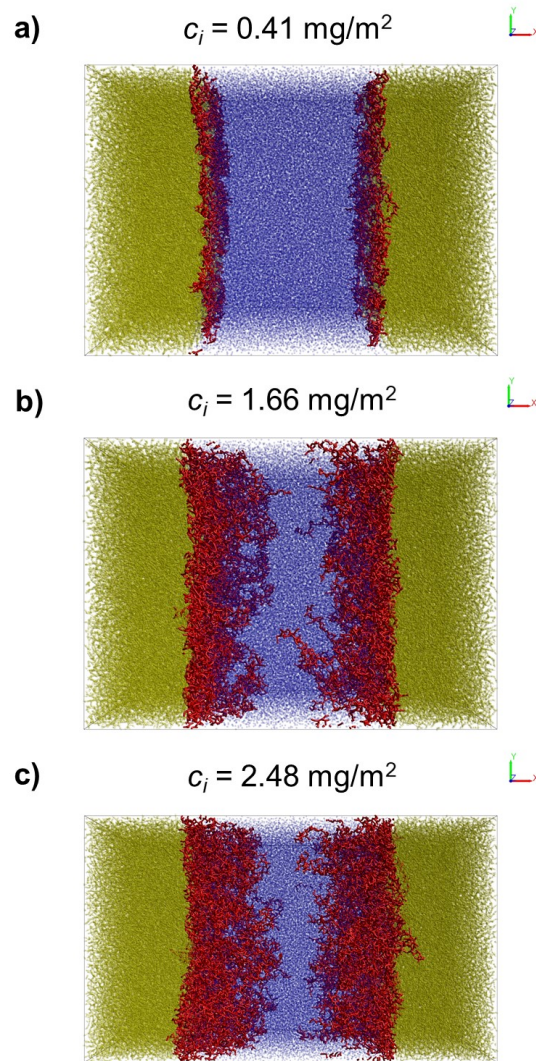


FIG. 4. Snapshots of equilibrated DPD boxes of the interface between oil (yellow) and water (blue) where Apovitellenin I (red) acts as the surfactant at increasing protein interface concentration,  $c_i$  (a, b, and c).

This is the author's peer reviewed, accepted manuscript. However, the online version of record will be different from this version once it has been copyedited and typeset.

PLEASE CITE THIS ARTICLE AS DOI: 10.1063/1.50079883

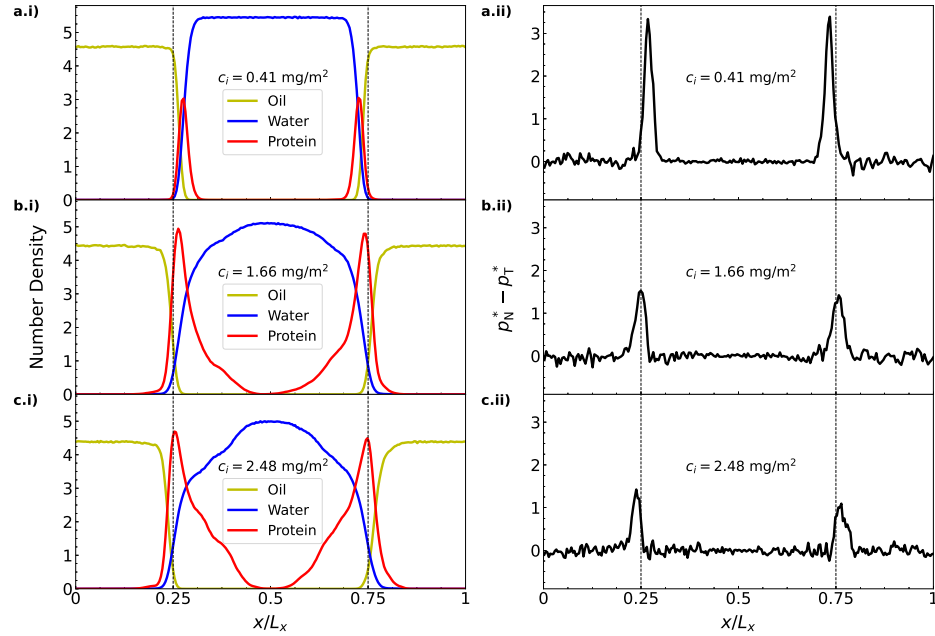


FIG. 5. Profiles of the number density of oil, water and protein (i) and of the difference between normal and tangential pressures,  $p_N^* - p_T^*$ , (ii) along the normalized  $x$ -direction normal to the interfaces at increasing protein interface concentrations (a, b, and c).

549 oil solution. Meanwhile, at increasing protein concentration, the mean radius of gyration of  
 550 Apovitellenin I at the interface decreases to a stable value and becomes comparable to that  
 551 in free solution. Thus, the packing mode of protein molecules at interface can be considered  
 552 similar to that observed in bulk phases, when the protein interface concentration is high.  
 553 Regarding the thickness of the protein layer (Figure 6a), it is directly derived from the width  
 554 of the protein density profile along the  $x$ -direction normal to the interface surface (see Fig-  
 555 ures 5i for reference). As expected, the protein layer thickness increase from 2 to 13 nm as  
 556 the protein interface concentration increases until the saturation of the interface where the  
 557 maximum and stable value for the thickness is reached. Fang and Dalglish<sup>106</sup> reported that  
 558 the adsorbed layer of casein molecules at the maximum coverage of the oil-water interface  
 559 was about 10 nm thick so that the protein molecules protrude further into the solution, as  
 560 also shown in this work (Figures 4 and 5i). Moreover, previous works<sup>107,108</sup> found that the



This is the author's peer reviewed, accepted manuscript. However, the online version of record will be different from this version once it has been copyedited and typeset.

PLEASE CITE THIS ARTICLE AS DOI: 10.1063/1.50079883

561 interfacial layer surrounding oil droplets in mayonnaise have an average thickness of around  
562 14 nm, which is comprised of surface-active proteins and lecithin-protein granules from egg  
563 yolk. Those findings are reasonably in accordance with our results. It is also straightforward  
564 to point out here that the emulsifier behaviour of only one LDL apoprotein is tested since it  
565 is identified as one of the most surface-active. LDL phospholipids may also have an effect on  
566 the interfacial tension of LDL-based emulsion by a further decrease of its saturation value.

568 In order to study the adsorption of Apovitellenin I at the oil-water interface, DPD simu-  
569 lations of a box containing two equidistant interface and one free protein molecule initially  
570 located in the center of the water phase were carried out. So, the protein diffusion from the  
571 aqueous environment towards the oil-water interface is investigated as represented in Figure  
572 7, where an illustrative example shows the three main steps of the protein adsorption mech-  
573 anism . First, the protein moves to the interface (a), then a portion of the molecule initiates  
574 the protein adsorption (b) and, after a certain time, Apovitellenin I is totally adsorbed at the  
575 oil-water interface (c). Apparently, there is no specific reason for the protein to be prefer-  
576 ably adsorbed at the right rather than at the left interface as the two sides are symmetrical.  
577 Moreover, the protein desorption has not been observed meaning that the adsorption process  
578 is most likely irreversible as also reported in previous experimental works.<sup>7,67</sup> To estimate  
579 the time required by a protein molecule to be fully absorbed as a function of its distance  
580 from the oil-water interface, multiple DPD simulations were performed by increasing the  
581 box size in the  $x$ -direction normal to the interfaces and the results are summarized in Figure  
582 8. Since the oil-to-water bead ratio is kept constant and the protein molecule is placed in  
583 the center of the water phase at the beginning of the simulation (see Figure 7 for reference),  
584 the abscissa of Figure 8 represents the initial distance between the geometric center of the  
585 protein molecule and the oil-water interface. The y-coordinate of Figure 8 expresses the time  
586 elapsed from the start of the simulation to the moment in which the protein molecule is to-  
587 tally adsorbed at one of the interfaces and it is estimated by visual inspection of simulation  
588 time frames. As also done in Figure 6, for each point three independent DPD simulations  
589 were carried out from which the mean value and the standard deviation were extracted.  
590 Although the error bars are relatively large, a linear trend passing through the origin of the  
591 axes can be identified in the range of investigated distances. The slope of  $0.978 \text{ ns}/\text{\AA}$  can  
592 be considered as an estimation of the required time of a liberated Apovitellenin I molecule  
593 to be totally adsorbed at a free interface as a function of their mutual distance.

This is the author's peer reviewed, accepted manuscript. However, the online version of record will be different from this version once it has been copyedited and typeset.

PLEASE CITE THIS ARTICLE AS DOI: 10.1063/5.0079883

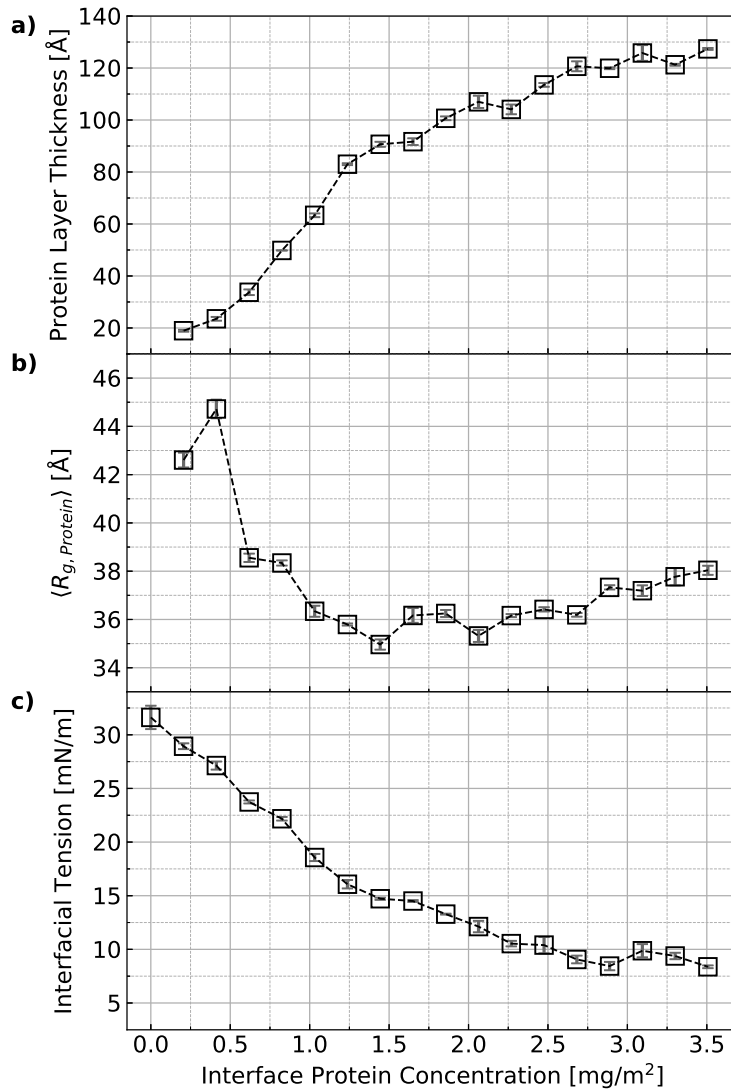


FIG. 6. Protein layer thickness (a), protein mean radius of gyration,  $\langle R_{g, Protein} \rangle$  (b), and interfacial tension (c) as a function of the interface concentration of Apovitellenin I. Error bars are estimated from three independent DPD simulations.

This is the author's peer reviewed, accepted manuscript. However, the online version of record will be different from this version once it has been copyedited and typeset.

PLEASE CITE THIS ARTICLE AS DOI: 10.1063/1.50079883

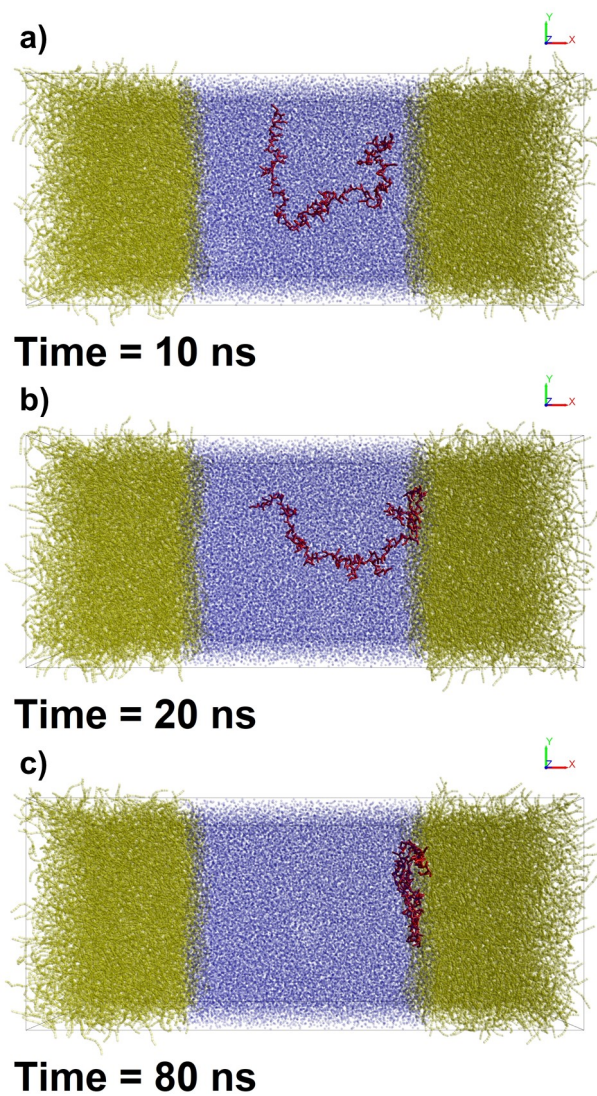


FIG. 7. Snapshots of the DPD simulation showing an illustrative example of the adsorption process of Apovitellenin I (one free molecule in red) at the interface between oil (yellow) and water (blue). The most significant steps of the adsorption mechanism are successively represented in a, b, and c.

This is the author's peer reviewed, accepted manuscript. However, the online version of record will be different from this version once it has been copyedited and typeset.

PLEASE CITE THIS ARTICLE AS DOI: 10.1063/1.50079883

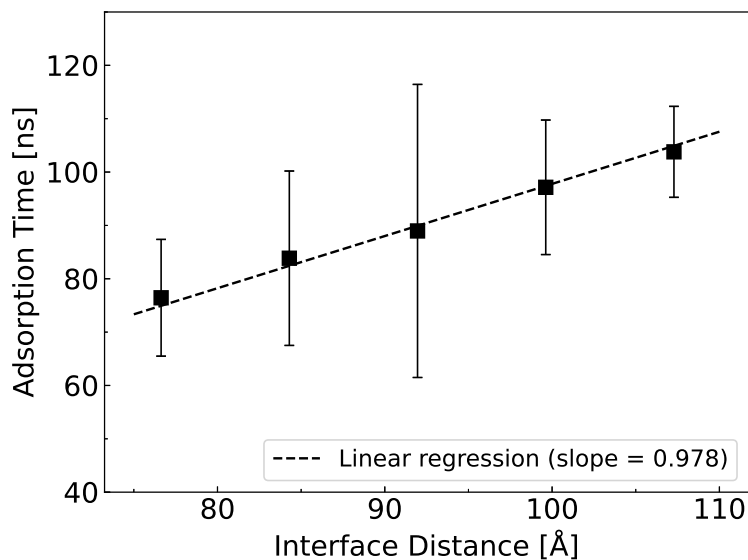


FIG. 8. Trend of the time required by one free molecule of Apovitellenin I to be fully adsorbed at the oil-water interface as a function of the initial distance between the protein geometric center and the oil-water interface. Error bars are estimated from three independent DPD simulations.

595 As already stated, LDL particles act as vectors of surfactant constituents (e.g., Apovitel-  
596 lenin I) that could not be soluble in water until they reach the interface. Therefore, a DPD  
597 simulation of a LDL-like particle with a lipid core surrounded by one molecule of Apovitel-  
598 lenin I was performed and the adsorption mechanism at the oil-water interface was tested.  
599 Although it is clear that this structure is far from being a realistic representation of a LDL  
600 particle, surprisingly the adsorption process proposed by Anton<sup>7</sup> is qualitatively reproduced  
601 as it can be seen in Figure 9 (Multimedia view). Indeed, first the LDL-like particle diffuses in  
602 the water bulk (a) until the protein situated on the particle surface comes into contact with  
603 the interface causing the unfolding of the LDL-like particle (b). Thus, the protein molecule  
604 initiates the LDL-like particle disruption by its anchorage at the oil-water interface. Then,  
605 the neutral lipids are released from the particle core and merge with the oil phase, while  
606 the protein molecule adsorbs at the interface (c). Since the system dimensions of Figure  
607 9 (Multimedia view) are the same of those represented in Figure 7, a general comparison  
608 can be made between two configurations, namely the liberated protein and the LDL-like

This is the author's peer reviewed, accepted manuscript. However, the online version of record will be different from this version once it has been copyedited and typeset.

PLEASE CITE THIS ARTICLE AS DOI: 10.1063/1.50079883

609 particle. In particular, the adsorption time of the LDL-like particle is significantly higher  
610 than that of the free protein. This can be intended as a greater stability of Apovitellenin I  
611 when surrounding the LDL-like particle rather than as a free molecule, also confirming that  
612 the liberated protein is supposed to be almost insoluble in water. Finally, it is important to  
613 remark that the representation of the LDL-like particle here presented must be considered  
614 qualitative, since both LDL size and its specific composition, namely including also the lipid  
615 distribution of the LDL core and all surfactant components situated on the LDL surface  
616 (e.g., phospholipids and other apoproteins), were not considered in the analysis.

This is the author's peer reviewed, accepted manuscript. However, the online version of record will be different from this version once it has been copyedited and typeset.

PLEASE CITE THIS ARTICLE AS DOI: 10.1063/1.50079883

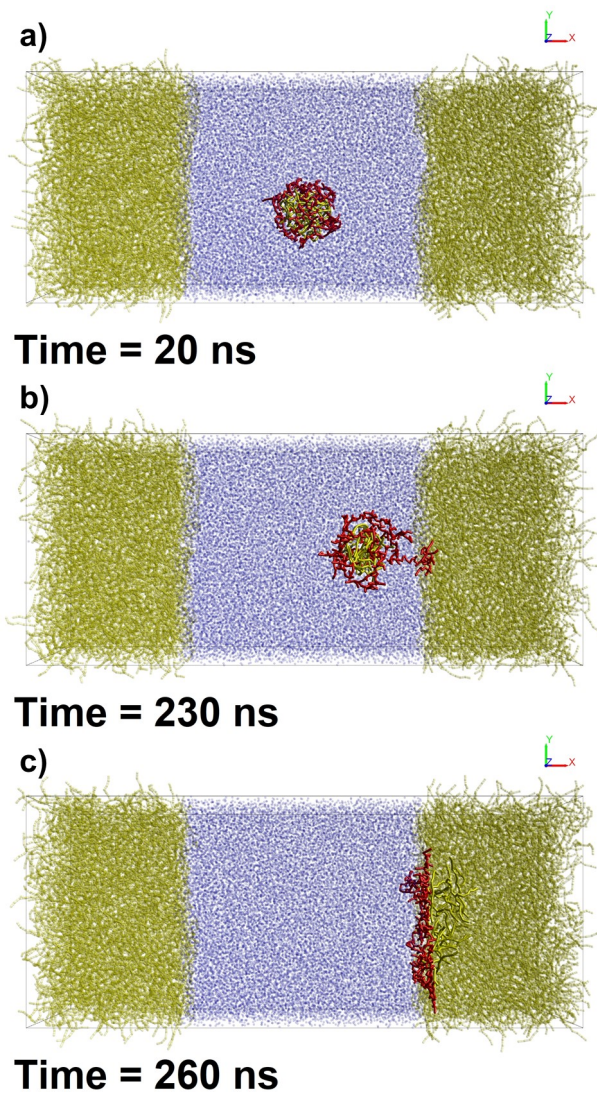


FIG. 9. Snapshots of the DPD simulation showing the adsorption process of a LDL-like particle with a lipid core (bright yellow) surrounded by one molecule of Apovitellenin I (red) at the interface between oil (yellow) and water (blue). The most significant steps of the adsorption mechanism are successively represented in a, b, and c (Multimedia view).

This is the author's peer reviewed, accepted manuscript. However, the online version of record will be different from this version once it has been copyedited and typeset.

PLEASE CITE THIS ARTICLE AS DOI: 10.1063/1.50079883

## 618 VI. CONCLUSIONS

619 Although egg yolk is widely used as an emulsifier in many food emulsion preparations,  
620 little experimental research on emulsifying properties of its individual components has been  
621 carried out since their extraction and isolation from the egg yolk complex matrix turned out  
622 to be difficult. Hence, this work focuses on the molecular model of an oil/water interface  
623 stabilized by one of the most surface-active protein of egg yolk LDLs, called Apovitellenin  
624 I. In order to take into account the system size, composition and the equilibration time  
625 needed by macro-molecules to re-arrange at interfaces, the molecular modeling technique  
626 here proposed is the Dissipative Particle Dynamics approach. Once the chemical species  
627 were determined, especially the biomolecule that should act as a surfactant at the oil/water  
628 interface, an automated coarse-graining procedure was carried out on the molecules involved  
629 in the ternary system. In DPD systems the intended physical properties are determined by  
630 means of a parameter calibration, which was here based on coupling DPD with all-atom  
631 Molecular Dynamics simulations of a single protein molecule in two different solvents, water  
632 and oil. Thus, both inter- and intra-molecular interactions employed in the DPD system  
633 are solely determined by matching the structural data from the atomistic simulations. The  
634 model was designed to test the most relevant physical properties of the protein studied,  
635 especially its emulsifier behavior. The results of MD and DPD simulations are compared in  
636 terms of protein structural and dynamics properties (radius of gyration, end-to-end distance,  
637 and diffusion coefficient), showing a good agreement between the two molecular techniques.  
638 Then, the oil-water interface system was simulated via the DPD technique. In particular, the  
639 present molecular modeling approach was able to properly describe the protein surfactant  
640 behavior by interfacial tension decrease at increasing protein surface concentration. The  
641 protein density profile, layer thickness, and adsorption time at the oil-water interface were  
642 also investigated, giving reasonable results in line with experimental evidence of similar pro-  
643 tein systems. In addition, the adsorption mechanism of an LDL-like particle is qualitatively  
644 reproduced. The modeling method here presented shows how computer molecular simula-  
645 tions can greatly help in the comprehension of food emulsion behavior and, in general, offer  
646 the advantage of estimating properties that are difficult to measure experimentally.

647 These results are encouraging and could be a starting point to explore the role of other  
648 surfactant molecules from egg yolk with an analogous molecular modeling method. More-

This is the author's peer reviewed, accepted manuscript. However, the online version of record will be different from this version once it has been copyedited and typeset.

PLEASE CITE THIS ARTICLE AS DOI: 10.1063/1.50079883

649 over, the main findings of this work together with non-equilibrium studies at the meso-scale  
650 will pave the way for a better understanding of the breakage and coalescence events of the  
651 oil droplets occurring in the food emulsion preparation. This information can be eventu-  
652 ally transferred to a computational fluid dynamics study coupled to a population balance  
653 model thus achieving a complete, general, and multi-scale digital twin of the food emulsion  
654 production process.

#### 655 SUPPLEMENTARY MATERIAL

656 See Supplementary Material for a further description of MD and DPD techniques used  
657 in this work.

#### 658 ACKNOWLEDGMENTS

659 This work was carried out in the context of the VIMMP project ([www.vimmp.eu](http://www.vimmp.eu)), where  
660 the entire workflow will contribute to populate a marketplace for generic multiscale and  
661 multiphysics simulations. The VIMMP project has received funding from the European  
662 Union's Horizon 2020 Research Innovation Programme under Grant Agreement n. 760907.  
663 We thank Dr. Piotr Pieczywek (Institute of Agrophysics, Polish Academy of Sciences,  
664 Doświadczalna 4, 20-270, Lublin, Poland) for sharing with us the MATLAB code for the  
665 water cluster algorithm employed in this work. We greatly appreciate the suggestion of a  
666 reviewer to include Figure 1.

#### 667 CONFLICT OF INTEREST

668 The authors have no conflicts to disclose.

#### 669 DATA AVAILABILITY

670 The data that support the findings of this study are openly available in Zenodo at <http://doi.org/10.5281/zenodo.5703247>, reference number 109.  
671



This is the author's peer reviewed, accepted manuscript. However, the online version of record will be different from this version once it has been copyedited and typeset.

PLEASE CITE THIS ARTICLE AS DOI: 10.1063/1.50079883

672 **REFERENCES**

- 673 <sup>1</sup>D. McClements, *Food Emulsions: Principles, Practice, and Techniques* (CRC Press, Boca  
674 Raton, FL, 2005).
- 675 <sup>2</sup>S. Friberg, J. Sjoblom, and K. Larsson, *Food Emulsions* (CRC Press, Boca Raton, FL,  
676 2003).
- 677 <sup>3</sup>A. Dubbelboer, J. Janssen, H. Hoogland, E. Zondervan, and J. Meuldijk, "Pilot-scale  
678 production process for high internal phase emulsions: Experimentation and modeling,"  
679 *Chemical Engineering Science* **148**, 32–43 (2016).
- 680 <sup>4</sup>A. Dubbelboer, *Towards optimization of emulsified consumer products : modeling and  
681 optimization of sensory and physicochemical aspects*, PhD dissertation, Technische Uni-  
682 versiteit Eindhoven, Department of Chemical Engineering and Chemistry (2016).
- 683 <sup>5</sup>S. Maindarkar, A. Dubbelboer, J. Meuldijk, H. Hoogland, and M. Henson, "Prediction  
684 of emulsion drop size distributions in colloid mills," *Chemical Engineering Science* **118**,  
685 114–125 (2014).
- 686 <sup>6</sup>P. Walstra, "Principles of emulsion formation," *Chemical Engineering Science* **48**, 333–349  
687 (1993).
- 688 <sup>7</sup>M. Anton, "Egg yolk: structures, functionalities and processes," *Journal of the Science  
689 of Food and Agriculture* **93**, 2871–2880 (2013).
- 690 <sup>8</sup>D. G. Dalgleish, "Food emulsions," in *Emulsions and emulsion stability*, edited by  
691 J. Sjoblom (Marcel Dekker Inc., 1996) p. 287–325.
- 692 <sup>9</sup>R. W. Burley, "Isolation and properties of a low-molecular-weight protein (apovitellenin  
693 I) from the high-lipid lipoprotein of emu egg yolk," *Biochemistry* **12**, 1464–1470 (1973).
- 694 <sup>10</sup>R. W. Burley, "Studies on the Apoproteins of the Major Lipoprotein of the Yolk of Hen's  
695 Eggs I. Isolation and Properties of the Low-molecular-weight Apoproteins." *Australian  
696 Journal of Biological Sciences* **28**, 121–132 (1975).
- 697 <sup>11</sup>W. Norde, *Colloids and Interfaces in Life Sciences and Bionanotechnology* (CRC Press,  
698 Boca Raton, FL, 2011).
- 699 <sup>12</sup>C.-A. Palma, M. Cecchini, and P. Samorì, "Predicting self-assembly: from empirism to  
700 determinism," *Chemical Society Reviews* **41**, 3713–3730 (2012).
- 701 <sup>13</sup>A. J. Stone, *The Theory of Intermolecular Forces* (Oxford University Press, Oxford, U.K.,  
702 2013).

This is the author's peer reviewed, accepted manuscript. However, the online version of record will be different from this version once it has been copyedited and typeset.

PLEASE CITE THIS ARTICLE AS DOI: 10.1063/1.50079883

- 703 <sup>14</sup>A. D. Lavino, M. Ferrari, A. A. Barresi, and D. Marchisio, “Effect of different good sol-  
704 vents in flash nano-precipitation via multi-scale population balance modeling-CFD cou-  
705 pling approach,” *Chemical Engineering Science* **245**, 116833 (2021).
- 706 <sup>15</sup>S. R. Euston, “Computer simulation of proteins: adsorption, gelation and self-  
707 association,” *Current Opinion in Colloid & Interface Science* **9**, 321–327 (2004).
- 708 <sup>16</sup>L. A. Pugaloni, E. Dickinson, R. Ettelaie, A. R. Mackie, and P. J. Wilde, “Competitive  
709 adsorption of proteins and low-molecular-weight surfactants: computer simulation and  
710 microscopic imaging,” *Advances in Colloid and Interface Science* **107**, 27–49 (2004).
- 711 <sup>17</sup>D. Zahn, “On the role of the solvent in biosystems: atomistic insights from computer  
712 simulations,” *Frontiers in Bioscience-Landmark* **14**, 3586–3593 (2009).
- 713 <sup>18</sup>E. Dickinson, “Structure and rheology of colloidal particle gels: Insight from computer  
714 simulation,” *Advances in Colloid and Interface Science* **199-200**, 114–127 (2013).
- 715 <sup>19</sup>S. Euston, “14 - Modelling and computer simulation of food structures,” in *Food Mi-  
716 crostructures*, Woodhead Publishing Series in Food Science, Technology and Nutrition,  
717 edited by V. Morris and K. Groves (Woodhead Publishing, 2013) pp. 336–385.
- 718 <sup>20</sup>A. Jusufi, “Molecular simulations of self-assembly processes of amphiphiles in dilute so-  
719 lutions: the challenge for quantitative modelling,” *Molecular Physics* **111**, 3182–3192  
720 (2013).
- 721 <sup>21</sup>J.-W. Handgraaf and F. Zerbetto, “Molecular dynamics study of onset of water gelation  
722 around the collagen triple helix,” *Proteins: Structure, Function, and Bioinformatics* **64**,  
723 711–718 (2006).
- 724 <sup>22</sup>A. D. Lavino, N. Di Pasquale, P. Carbone, and D. L. Marchisio, “A novel multiscale model  
725 for the simulation of polymer flash nano-precipitation,” *Chemical Engineering Science*  
726 **171**, 485–494 (2017).
- 727 <sup>23</sup>A. D. Lavino, P. Carbone, and D. Marchisio, “MARTINI coarse-grained model for poly- $\epsilon$ -  
728 caprolactone in acetone-water mixtures,” *The Canadian Journal of Chemical Engineering*  
729 **98**, 1868–1879 (2020).
- 730 <sup>24</sup>A. D. Lavino, L. Banetta, P. Carbone, and D. L. Marchisio, “Extended Charge-On-  
731 Particle Optimized Potentials for Liquid Simulation Acetone Model: The Case of Ace-  
732 tone–Water Mixtures,” *The Journal of Physical Chemistry B* **122**, 5234–5241 (2018).
- 733 <sup>25</sup>D. Frenkel and B. Smit, *Understanding Molecular Simulation*, 2nd ed. (Academic Press,  
734 Inc., USA, 2001).

This is the author's peer reviewed, accepted manuscript. However, the online version of record will be different from this version once it has been copyedited and typeset.

PLEASE CITE THIS ARTICLE AS DOI: 10.1063/5.0079883

- 735 <sup>26</sup>C. J. Cramer, *Essentials of Computational Chemistry: Theories and Models*, 2nd ed.  
736 (Wiley, New York, 2004).
- 737 <sup>27</sup>P. J. Hoogerbrugge and J. M. V. A. Koelman, “Simulating Microscopic Hydrodynamic  
738 Phenomena with Dissipative Particle Dynamics,” *Europhysics Letters (EPL)* **19**, 155–160  
739 (1992).
- 740 <sup>28</sup>P. Español and P. Warren, “Statistical Mechanics of Dissipative Particle Dynamics,”  
741 *Europhysics Letters (EPL)* **30**, 191–196 (1995).
- 742 <sup>29</sup>R. D. Groot and P. B. Warren, “Dissipative particle dynamics: Bridging the gap between  
743 atomistic and mesoscopic simulation,” *The Journal of Chemical Physics* **107**, 4423–4435  
744 (1997).
- 745 <sup>30</sup>N. Lauriello, J. Kondracki, A. Buffo, G. Boccardo, M. Bouaifi, M. Lisal, and D. Marchisio,  
746 “Simulation of high Schmidt number fluids with dissipative particle dynamics: Parameter  
747 identification and robust viscosity evaluation,” *Physics of Fluids* **33**, 073106 (2021).
- 748 <sup>31</sup>E. Dickinson and S. R. Euston, “Monte Carlo simulation of colloidal systems,” *Advances  
749 in Colloid and Interface Science* **42**, 89–148 (1992).
- 750 <sup>32</sup>R. E. Anderson, V. S. Pande, and C. J. Radke, “Dynamic lattice Monte Carlo simulation  
751 of a model protein at an oil/water interface,” *The Journal of Chemical Physics* **112**,  
752 9167–9185 (2000).
- 753 <sup>33</sup>G. Dalkas and S. R. Euston, “Molecular simulation of protein adsorption and conformation  
754 at gas-liquid, liquid-liquid and solid-liquid interfaces,” *Current Opinion in Colloid &  
755 Interface Science* **41**, 1–10 (2019).
- 756 <sup>34</sup>D. Zare, K. M. McGrath, and J. R. Allison, “Deciphering  $\beta$ -Lactoglobulin Interactions  
757 at an Oil–Water Interface: A Molecular Dynamics Study,” *Biomacromolecules* **16**, 1855–  
758 1861 (2015).
- 759 <sup>35</sup>D. Zare, J. R. Allison, and K. M. McGrath, “Molecular Dynamics Simulation of  
760  $\beta$ -Lactoglobulin at Different Oil/Water Interfaces,” *Biomacromolecules* **17**, 1572–1581  
761 (2016).
- 762 <sup>36</sup>D. L. Cheung, “Adsorption and conformations of lysozyme and  $\alpha$ -lactalbumin at a water-  
763 octane interface,” *The Journal of Chemical Physics* **147**, 195101 (2017).
- 764 <sup>37</sup>D. L. Cheung, “Conformations of Myoglobin-Derived Peptides at the Air–Water Inter-  
765 face,” *Langmuir* **32**, 4405–4414 (2016).

This is the author's peer reviewed, accepted manuscript. However, the online version of record will be different from this version once it has been copyedited and typeset.

PLEASE CITE THIS ARTICLE AS DOI: 10.1063/1.50079883

- 766 <sup>38</sup>S. R. Euston, “Molecular Dynamics Simulation of Protein Adsorption at Fluid Interfaces:  
767 A Comparison of All-Atom and Coarse-Grained Models,” *Biomacromolecules* **11**, 2781–  
768 2787 (2010).
- 769 <sup>39</sup>S. R. Euston, P. Hughes, M. A. Naser, and R. E. Westacott, “Comparison of the Adsorbed  
770 Conformation of Barley Lipid Transfer Protein at the Decane-Water and Vacuum-Water  
771 Interface: A Molecular Dynamics Simulation,” *Biomacromolecules* **9**, 1443–1453 (2008).
- 772 <sup>40</sup>S. R. Euston, P. Hughes, M. A. Naser, and R. E. Westacott, “Molecular Dynamics  
773 Simulation of the Cooperative Adsorption of Barley Lipid Transfer Protein and cis-  
774 Isocohumulone at the Vacuum-Water Interface,” *Biomacromolecules* **9**, 3024–3032 (2008).
- 775 <sup>41</sup>F. Sepehr and S. J. Paddison, “Dissipative Particle Dynamics interaction parameters from  
776 *ab initio* calculations,” *Chemical Physics Letters* **645**, 20–26 (2016).
- 777 <sup>42</sup>H. Lei, B. Caswell, and G. E. Karniadakis, “Direct construction of mesoscopic models  
778 from microscopic simulations,” *Physical Review E* **81**, 026704 (2010).
- 779 <sup>43</sup>W. Tschöp, K. Kremer, J. Batoulis, T. Bürger, and O. Hahn, “Simulation of poly-  
780 mer melts. I. Coarse-graining procedure for polycarbonates,” *Acta Polymerica* **49**, 61–74  
781 (1998).
- 782 <sup>44</sup>A. Vishnyakov and A. V. Neimark, “Self-Assembly in Nafion Membranes upon Hydration:  
783 Water Mobility and Adsorption Isotherms,” *The Journal of Physical Chemistry B* **118**,  
784 11353–11364 (2014).
- 785 <sup>45</sup>K. Patterson, M. Lisal, and C. M. Colina, “Adsorption behavior of model proteins on  
786 surfaces,” *Fluid Phase Equilibria* **302**, 48–54 (2011).
- 787 <sup>46</sup>A. Vishnyakov, D. S. Talaga, and A. V. Neimark, “DPD Simulation of Protein Confor-  
788 mations: From  $\alpha$ -Helices to  $\beta$ -Structures,” *The Journal of Physical Chemistry Letters* **3**,  
789 3081–3087 (2012).
- 790 <sup>47</sup>K. Okuwaki, H. Doi, K. Fukuzawa, and Y. Mochizuki, “Folding simulation of small pro-  
791 teins by dissipative particle dynamics (DPD) with non-empirical interaction parameters  
792 based on fragment molecular orbital calculations,” *Applied Physics Express* **13**, 017002  
793 (2019).
- 794 <sup>48</sup>M. Ndao, F. Goujon, A. Ghoufi, and P. Malfreyt, “Coarse-grained modeling of the  
795 oil–water–surfactant interface through the local definition of the pressure tensor and in-  
796 terfacial tension,” *Theoretical Chemistry Accounts* **136**, 21 (2017).

This is the author's peer reviewed, accepted manuscript. However, the online version of record will be different from this version once it has been copyedited and typeset.

PLEASE CITE THIS ARTICLE AS DOI: 10.1063/1.50079883

- 797 <sup>49</sup>A. Ghoufi, P. Malfreyt, and D. J. Tildesley, "Computer modelling of the surface tension  
798 of the gas-liquid and liquid-liquid interface," *Chemical Society Reviews* **45**, 1387-1409  
799 (2016).
- 800 <sup>50</sup>A. Khedr and A. Striolo, "DPD Parameters Estimation for Simultaneously Simulating  
801 Water-Oil Interfaces and Aqueous Nonionic Surfactants," *Journal of Chemical Theory  
802 and Computation* **14**, 6460-6471 (2018).
- 803 <sup>51</sup>A. Maiti and S. McGrother, "Bead-bead interaction parameters in dissipative particle  
804 dynamics: Relation to bead-size, solubility parameter, and surface tension," *The Journal  
805 of Chemical Physics* **120**, 1594-1601 (2004).
- 806 <sup>52</sup>S.-l. Lin, M.-y. Xu, and Z.-r. Yang, "Dissipative particle dynamics study on the mesostruc-  
807 tures of n-octadecane/water emulsion with alternating styrene-maleic acid copolymers as  
808 emulsifier," *Soft Matter* **8**, 375-384 (2012).
- 809 <sup>53</sup>F. Alvarez, E. A. Flores, L. V. Castro, J. G. Hernández, A. López, and F. Vázquez, "Dis-  
810 sipative Particle Dynamics (DPD) Study of Crude Oil-Water Emulsions in the Presence  
811 of a Functionalized Co-polymer," *Energy & Fuels* **25**, 562-567 (2011).
- 812 <sup>54</sup>L. Rekvig, B. Hafskjold, and B. Smit, "Molecular Simulations of Surface Forces and Film  
813 Rupture in Oil/Water/Surfactant Systems," *Langmuir* **20**, 11583-11593 (2004).
- 814 <sup>55</sup>E. G. Perkins, "Chapter 2 - composition of soybeans and soybean products," in *Practical  
815 Handbook of Soybean Processing and Utilization*, edited by D. R. Erickson (AOCS Press,  
816 1995) pp. 9-28.
- 817 <sup>56</sup>J. Leaver and D. G. Dalgleish, "Variations in the binding of  $\beta$ -casein to oil-water interfaces  
818 detected by trypsin-catalysed hydrolysis," *Journal of Colloid and Interface Science* **149**,  
819 49-55 (1992).
- 820 <sup>57</sup>R. Xiong, G. Xie, and A. Edmondson, "Modelling the pH of mayonnaise by the ratio of  
821 egg to vinegar," *Food Control* **11**, 49-56 (2000).
- 822 <sup>58</sup>M. Anton and G. Gandemer, "Composition, Solubility and Emulsifying Properties of  
823 Granules and Plasma of Egg Yolk," *Journal of Food Science* **62**, 484-487 (1997).
- 824 <sup>59</sup>J. N. Dyer-Hurdon and I. A. Nnanna, "Cholesterol Content and Functionality of Plasma  
825 and Granules Fractionated from Egg Yolk," *Journal of Food Science* **58**, 1277-1281 (1993).
- 826 <sup>60</sup>M. Le Denmat, M. Anton, and V. Beaumal, "Characterisation of emulsion properties  
827 and of interface composition in O/W emulsions prepared with hen egg yolk, plasma and  
828 granules," *Food Hydrocolloids* **14**, 539-549 (2000).

This is the author's peer reviewed, accepted manuscript. However, the online version of record will be different from this version once it has been copyedited and typeset.

PLEASE CITE THIS ARTICLE AS DOI: 10.1063/1.50079883

- 829 <sup>61</sup>V. Martinet, V. Beaumal, M. Dalgarrondo, and M. Anton, “Emulsifying properties and  
830 adsorption behavior of egg yolk lipoproteins (LDL and HDL) in oil-in-water emulsions,”  
831 in *Food emulsions and dispersions*, edited by M. Anton (Research Signpost, Trivandrum,  
832 2002) p. 103–116.
- 833 <sup>62</sup>W. Cook and W. Martin, “Egg lipoproteins,” in *Structural and Functional Aspects of*  
834 *Lipoproteins in Living Systems*, edited by E. Tria and A. Scanu (Academic Press, London,  
835 1969) p. 579–615.
- 836 <sup>63</sup>R. W. Burley and W. H. Cook, “Isolation and composition of avian egg yolk granules and  
837 their constituent  $\alpha$ - and  $\beta$ -lipovitellins,” *Canadian Journal of Biochemistry and Physiol-*  
838 *ogy* **39**, 1295–1307 (1961).
- 839 <sup>64</sup>P. Jolivet, C. Boulard, V. Beaumal, T. Chardot, and M. Anton, “Protein components  
840 of low-density lipoproteins purified from hen egg yolk,” *Journal of Agricultural and Food*  
841 *Chemistry* **54**, 4424–4429 (2006).
- 842 <sup>65</sup>P. Jolivet, C. Boulard, T. Chardot, and M. Anton, “New Insights into the Structure of  
843 Apolipoprotein B from Low-Density Lipoproteins and Identification of a Novel YGP-like  
844 Protein in Hen Egg Yolk,” *Journal of Agricultural and Food Chemistry* **56**, 5871–5879  
845 (2008).
- 846 <sup>66</sup>R. J. Evans, D. H. Bauer, S. L. Bandemer, S. B. Vaghefi, and C. J. Flegal, “Structure of  
847 egg yolk very low density lipoprotein. polydispersity of the very low density lipoprotein  
848 and the role of lipovitellenin in the structure,” *Archives of Biochemistry and Biophysics*  
849 **154**, 493–500 (1973).
- 850 <sup>67</sup>M. Anton, V. Martinet, M. Dalgarrondo, V. Beaumal, E. David-Briand, and H. Rabes-  
851 ona, “Chemical and structural characterisation of low-density lipoproteins purified from  
852 hen egg yolk,” *Food Chemistry* **83**, 175–183 (2003).
- 853 <sup>68</sup>V. Martinet, P. Saulnier, V. Beaumal, J.-L. Courthaudon, and M. Anton, “Surface  
854 properties of hen egg yolk low-density lipoproteins spread at the air–water interface,”  
855 *Colloids and Surfaces B: Biointerfaces* **31**, 185–194 (2003).
- 856 <sup>69</sup>S. Dauphas, V. Beaumal, A. Riaublanc, and M. Anton, “Hen egg yolk low-density lipopro-  
857 teins film spreading at the air-water and oil-water interfaces,” *Journal of Agricultural and*  
858 *Food Chemistry* **54**, 3733–3737 (2006).
- 859 <sup>70</sup>S. Dauphas, V. Beaumal, P. Gunning, A. Mackie, P. Wilde, V. Vié, A. Riaublanc, and  
860 M. Anton, “Structures and rheological properties of hen egg yolk low density lipopro-

This is the author's peer reviewed, accepted manuscript. However, the online version of record will be different from this version once it has been copyedited and typeset.

PLEASE CITE THIS ARTICLE AS DOI: 10.1063/1.50079883

- 861 tein layers spread at the air–water interface at pH 3 and 7,” *Colloids and Surfaces B:*  
862 *Biointerfaces* **57**, 124–133 (2007).
- 863 <sup>71</sup>S. Dauphas, V. Beaumal, P. Gunning, A. Mackie, P. Wilde, V. Vié, A. Riaublanc, and  
864 M. Anton, “Structure modification in hen egg yolk low density lipoproteins layers between  
865 30 and 45mN/m observed by AFM,” *Colloids and Surfaces B: Biointerfaces* **54**, 241–248  
866 (2007).
- 867 <sup>72</sup>The UniProt Consortium, “Uniprot: the universal protein knowledgebase in 2021,” *Nu-*  
868 *cleic Acids Research* **49**, D480–D489 (2020).
- 869 <sup>73</sup>M. Allen and D. Tildesley, *Computer Simulation of Liquids*, 2nd ed. (Oxford University  
870 Press, Oxford, U.K., 2017).
- 871 <sup>74</sup>E. Moeendarbary, T. Y. Ng, and M. Zangeneh, “Dissipative particle dynamics: Intro-  
872 duction, methodology and complex fluid applications — A review,” *International Journal*  
873 *of Applied Mechanics* **01**, 737–763 (2009).
- 874 <sup>75</sup>D. R. Lide, ed., *CRC Handbook of Chemistry and Physics*, 85th ed. (CRC press, Boca  
875 Raton, FL, 2005).
- 876 <sup>76</sup>W. L. Jorgensen and J. Tirado-Rives, “The OPLS [optimized potentials for liquid simula-  
877 tions] potential functions for proteins, energy minimizations for crystals of cyclic peptides  
878 and crambin,” *Journal of the American Chemical Society* **110**, 1657–1666 (1988).
- 879 <sup>77</sup>W. L. Jorgensen, D. S. Maxwell, and J. Tirado-Rives, “Development and Testing of  
880 the OPLS All-Atom Force Field on Conformational Energetics and Properties of Organic  
881 Liquids,” *Journal of the American Chemical Society* **118**, 11225–11236 (1996).
- 882 <sup>78</sup>W. L. Jorgensen, J. Chandrasekhar, J. D. Madura, R. W. Impey, and M. L. Klein,  
883 “Comparison of simple potential functions for simulating liquid water,” *The Journal of*  
884 *Chemical Physics* **79**, 926–935 (1983).
- 885 <sup>79</sup>U. Essmann, L. Perera, M. L. Berkowitz, T. Darden, H. Lee, and L. G. Pedersen, “A  
886 smooth particle mesh Ewald method,” *The Journal of Chemical Physics* **103**, 8577–8593  
887 (1995).
- 888 <sup>80</sup>H. J. C. Berendsen, J. P. M. Postma, W. F. van Gunsteren, A. DiNola, and J. R. Haak,  
889 “Molecular dynamics with coupling to an external bath,” *The Journal of Chemical Physics*  
890 **81**, 3684–3690 (1984).
- 891 <sup>81</sup>J. G. E. M. Fraaije, J. van Male, P. Becherer, and R. Serral Gracià, “Coarse-grained mod-  
892 els for automated fragmentation and parametrization of molecular databases,” *Journal of*

This is the author's peer reviewed, accepted manuscript. However, the online version of record will be different from this version once it has been copyedited and typeset.

PLEASE CITE THIS ARTICLE AS DOI: 10.1063/5.0079883

- 893 Chemical Information and Modeling **56**, 2361–2377 (2016).
- 894 <sup>82</sup>M. Diedenhofen and A. Klamt, “COSMO-RS as a tool for property prediction of IL  
895 mixtures—A review,” *Fluid Phase Equilibria* **294**, 31–38 (2010).
- 896 <sup>83</sup>A. Klamt, *COSMO-RS: From Quantum Chemistry to Fluid Phase Thermodynamics and  
897 Drug Design* (Elsevier, Amsterdam, 2005).
- 898 <sup>84</sup>A. Jakalian, B. L. Bush, D. B. Jack, and C. I. Bayly, “Fast, efficient generation of  
899 high-quality atomic charges. AM1-BCC model: I. Method,” *Journal of Computational  
900 Chemistry* **21**, 132–146 (2000).
- 901 <sup>85</sup>A. Jakalian, D. B. Jack, and C. I. Bayly, “Fast, efficient generation of high-quality  
902 atomic charges. AM1-BCC model: II. Parameterization and validation,” *Journal of Com-  
903 putational Chemistry* **23**, 1623–1641 (2002).
- 904 <sup>86</sup>P. C. Petris, P. Becherer, and J. G. E. M. Fraaije, “Alkane/Water Partition Coefficient  
905 Calculation Based on the Modified AM1 Method and Internal Hydrogen Bonding Sam-  
906 pling Using COSMO-RS,” *Journal of Chemical Information and Modeling* **61**, 3453–3462  
907 (2021).
- 908 <sup>87</sup>A. K. Rappe and W. A. Goddard, “Charge equilibration for molecular dynamics simula-  
909 tions,” *The Journal of Physical Chemistry* **95**, 3358–3363 (1991).
- 910 <sup>88</sup>P. M. Pieczywek, W. Płaziński, and A. Zdunek, “Dissipative particle dynamics model  
911 of homogalacturonan based on molecular dynamics simulations,” *Scientific Reports* **10**,  
912 14691 (2020).
- 913 <sup>89</sup>K. R. Hadley and C. McCabe, “On the Investigation of Coarse-Grained Models for Water:  
914 Balancing Computational Efficiency and the Retention of Structural Properties,” *The  
915 Journal of Physical Chemistry B* **114**, 4590–4599 (2010).
- 916 <sup>90</sup>E. Zohravi, E. Shirani, and A. Pischevar, “Influence of the conservative force on transport  
917 coefficients in the DPD method,” *Molecular Simulation* **44**, 254–261 (2018).
- 918 <sup>91</sup>A. G. Gaonkar, “Effects of salt, temperature, and surfactants on the interfacial tension  
919 behavior of a vegetable oil/water system,” *Journal of Colloid and Interface Science* **149**,  
920 256–260 (1992).
- 921 <sup>92</sup>D. Reith, H. Meyer, and F. Müller-Plathe, “Mapping Atomistic to Coarse-Grained Poly-  
922 mer Models Using Automatic Simplex Optimization To Fit Structural Properties,” *Macro-  
923 molecules* **34**, 2335–2345 (2001).



This is the author's peer reviewed, accepted manuscript. However, the online version of record will be different from this version once it has been copyedited and typeset.

PLEASE CITE THIS ARTICLE AS DOI: 10.1063/1.50079883

- 924 <sup>93</sup>Y. Li, B. C. Abberton, M. Kröger, and W. K. Liu, “Challenges in Multiscale Modeling  
925 of Polymer Dynamics,” *Polymers* **5**, 751–832 (2013).
- 926 <sup>94</sup>V. Agrawal, G. Arya, and J. Oswald, “Simultaneous Iterative Boltzmann Inversion for  
927 Coarse-Graining of Polyurea,” *Macromolecules* **47**, 3378–3389 (2014).
- 928 <sup>95</sup>J. G. E. M. Fraaije, J. van Male, P. Becherer, and R. Serral Gracià, “Calculation  
929 of Diffusion Coefficients through Coarse-Grained Simulations Using the Automated-  
930 Fragmentation-Parametrization Method and the Recovery of Wilke–Chang Statistical  
931 Correlation,” *Journal of Chemical Theory and Computation* **14**, 479–485 (2018).
- 932 <sup>96</sup>M. E. Young, P. A. Carroad, and R. L. Bell, “Estimation of diffusion coefficients of  
933 proteins,” *Biotechnology and Bioengineering* **22**, 947–955 (1980).
- 934 <sup>97</sup>M. T. Tyn and T. W. Gusek, “Prediction of diffusion coefficients of proteins,” *Biotech-  
935 nology and Bioengineering* **35**, 327–338 (1990).
- 936 <sup>98</sup>L. He and B. Niemeyer, “A Novel Correlation for Protein Diffusion Coefficients Based on  
937 Molecular Weight and Radius of Gyration,” *Biotechnology Progress* **19**, 544–548 (2003).
- 938 <sup>99</sup>J. Kestin, M. Sokolov, and W. A. Wakeham, “Viscosity of liquid water in the range -8°C  
939 to 150°C,” *Journal of Physical and Chemical Reference Data* **7**, 941–948 (1978).
- 940 <sup>100</sup>F. C. Magne and E. L. Skau, “Viscosities and Densities of Solvent-Vegetable Oil Mix-  
941 tures,” *Industrial & Engineering Chemistry* **37**, 1097–1101 (1945).
- 942 <sup>101</sup>J. H. Irving and J. G. Kirkwood, “The statistical mechanical theory of transport processes.  
943 iv. the equations of hydrodynamics,” *The Journal of Chemical Physics* **18**, 817–829 (1950).
- 944 <sup>102</sup>Culgi B.V., The Netherlands, “The Chemistry Unified Language Interface (CULGI),”  
945 [www.culgi.com](http://www.culgi.com) (2020), version 13.0.0.
- 946 <sup>103</sup>T. P. Hill and J. Miller, “How to combine independent data sets for the same quantity,”  
947 *Chaos: An Interdisciplinary Journal of Nonlinear Science* **21**, 033102 (2011).
- 948 <sup>104</sup>E. K. Peter, K. Lykov, and I. V. Pivkin, “A polarizable coarse-grained protein model  
949 for dissipative particle dynamics,” *Physical Chemistry Chemical Physics* **17**, 24452–24461  
950 (2015).
- 951 <sup>105</sup>J. Wang and T. Hou, “Application of molecular dynamics simulations in molecular prop-  
952 erty prediction II: Diffusion coefficient,” *Journal of Computational Chemistry* **32**, 3505–  
953 3519 (2011).
- 954 <sup>106</sup>Y. Fang and D. G. Dalgleish, “Dimensions of the Adsorbed Layers in Oil-in-Water Emul-  
955 sions Stabilized by Caseins,” *Journal of Colloid and Interface Science* **156**, 329–334 (1993).

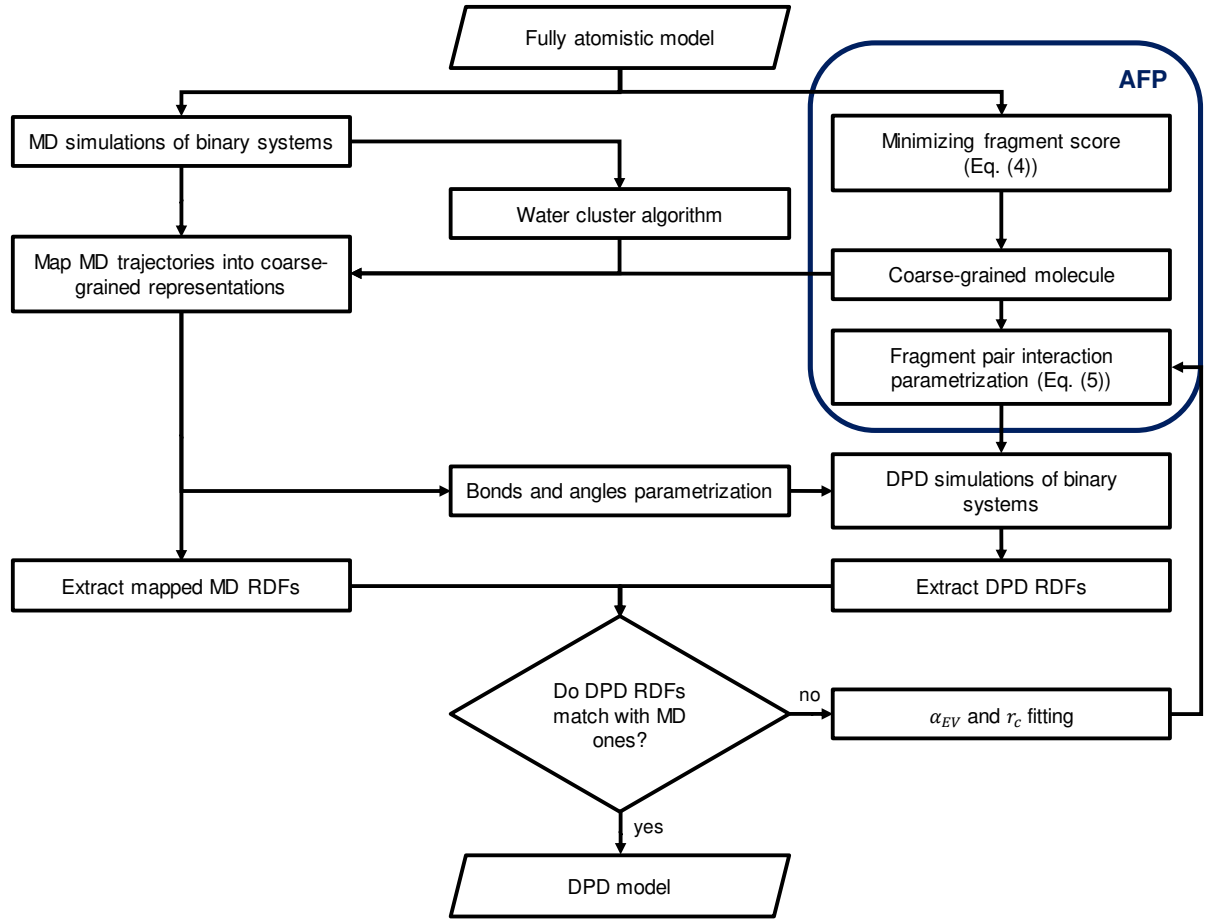
This is the author's peer reviewed, accepted manuscript. However, the online version of record will be different from this version once it has been copyedited and typeset.

PLEASE CITE THIS ARTICLE AS DOI: 10.1063/5.0079883

- 956 <sup>107</sup>L. Ford, R. Borwankar, R. Martin, and D. Holcomb, “Dressings and sauces,” in *Food*  
957 *Emulsions*, edited by S. Friberg and K. Larsson (Marcel Dekker, New York, 1997) 3rd  
958 ed., pp. 361–412.
- 959 <sup>108</sup>M. Langton, E. Jordansson, A. Altskär, C. Sørensen, and A.-M. Hermansson, “Mi-  
960 crostructure and image analysis of mayonnaises,” *Food Hydrocolloids* **13**, 113–125 (1999).
- 961 <sup>109</sup>M. Ferrari, J.-W. Handgraaf, G. Boccardo, A. Buffo, M. Vanni, and D. L. Marchisio,  
962 “Dataset for “Molecular modeling of the interface of an egg yolk protein-based emulsion” ,”  
963 Zenodo (2021), Dataset, <https://doi.org/10.5281/zenodo.5703247>.

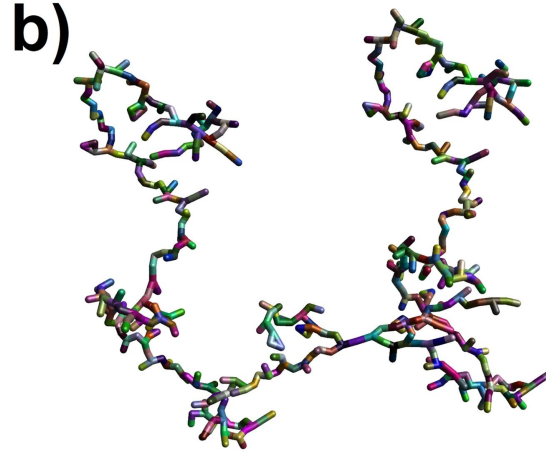
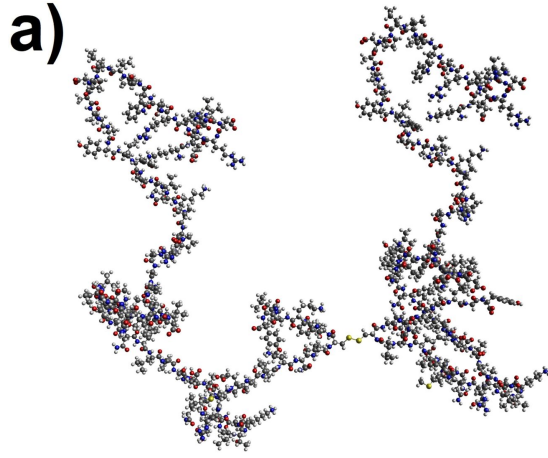
This is the author's peer reviewed, accepted manuscript. However, the online version of record will be different from this version once it has been copyedited and typeset.

PLEASE CITE THIS ARTICLE AS DOI: 10.1063/1.50079883



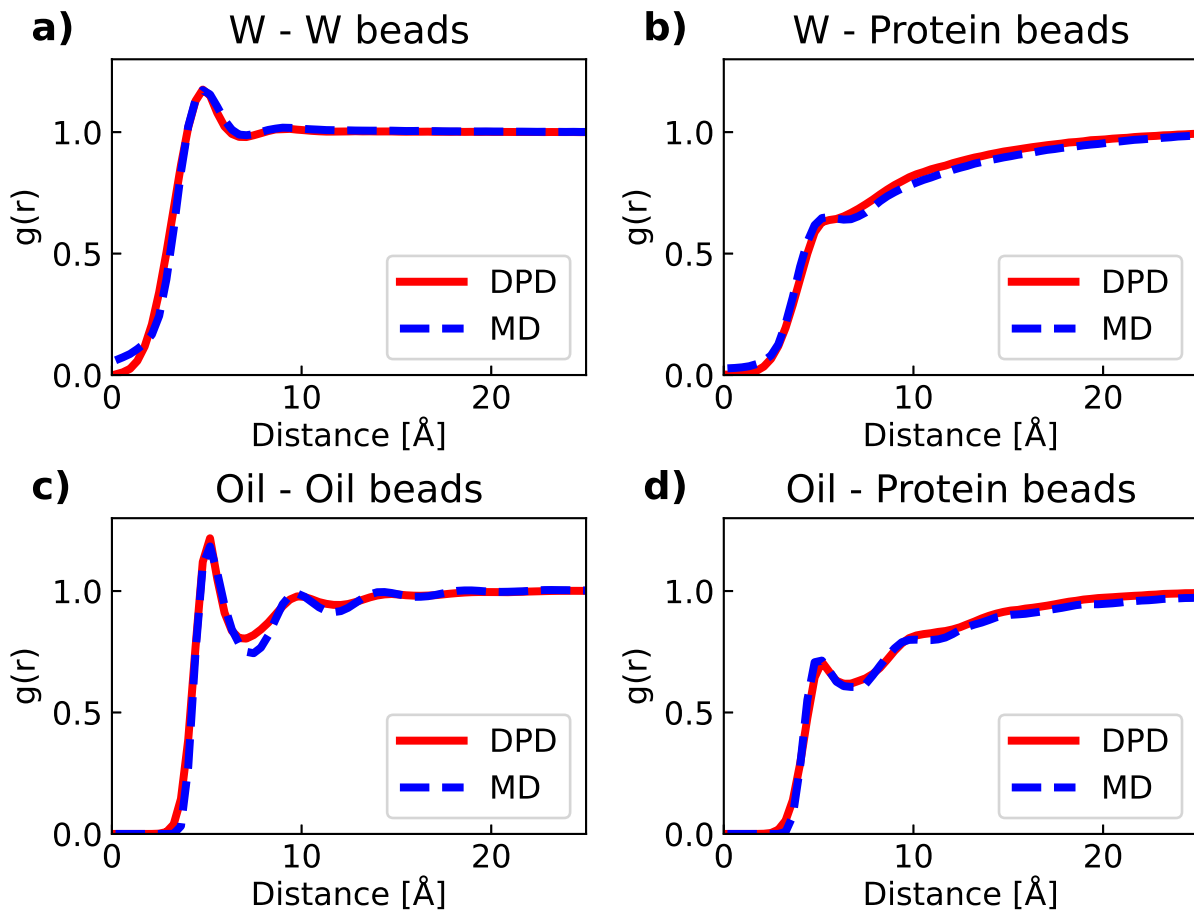
This is the author's peer reviewed, accepted manuscript. However, the online version of record will be different from this version once it has been copyedited and typeset.

PLEASE CITE THIS ARTICLE AS DOI: 10.1063/1.50079883



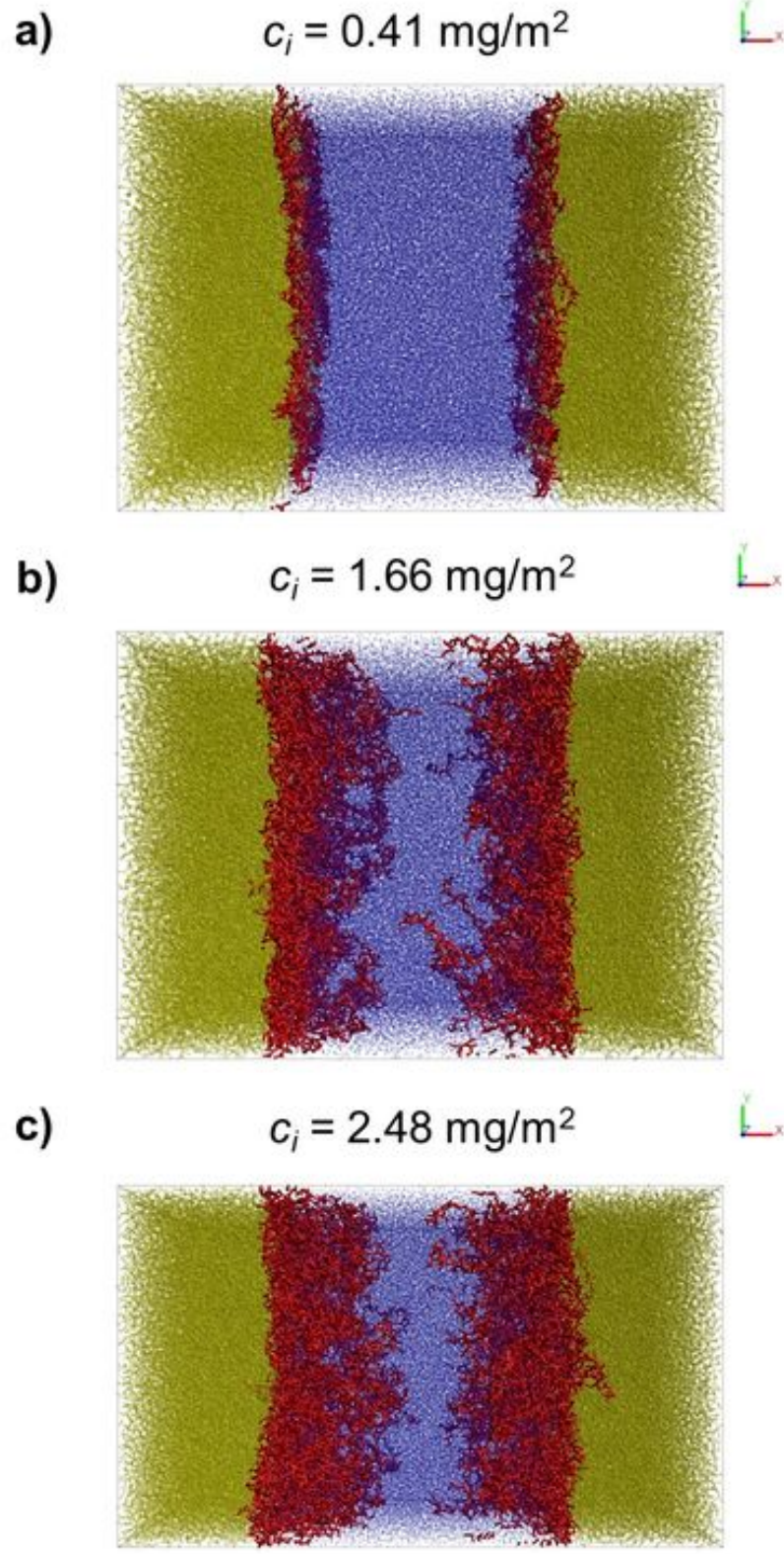
This is the author's peer reviewed, accepted manuscript. However, the online version of record will be different from this version once it has been copyedited and typeset.

PLEASE CITE THIS ARTICLE AS DOI: 10.1063/5.0079883



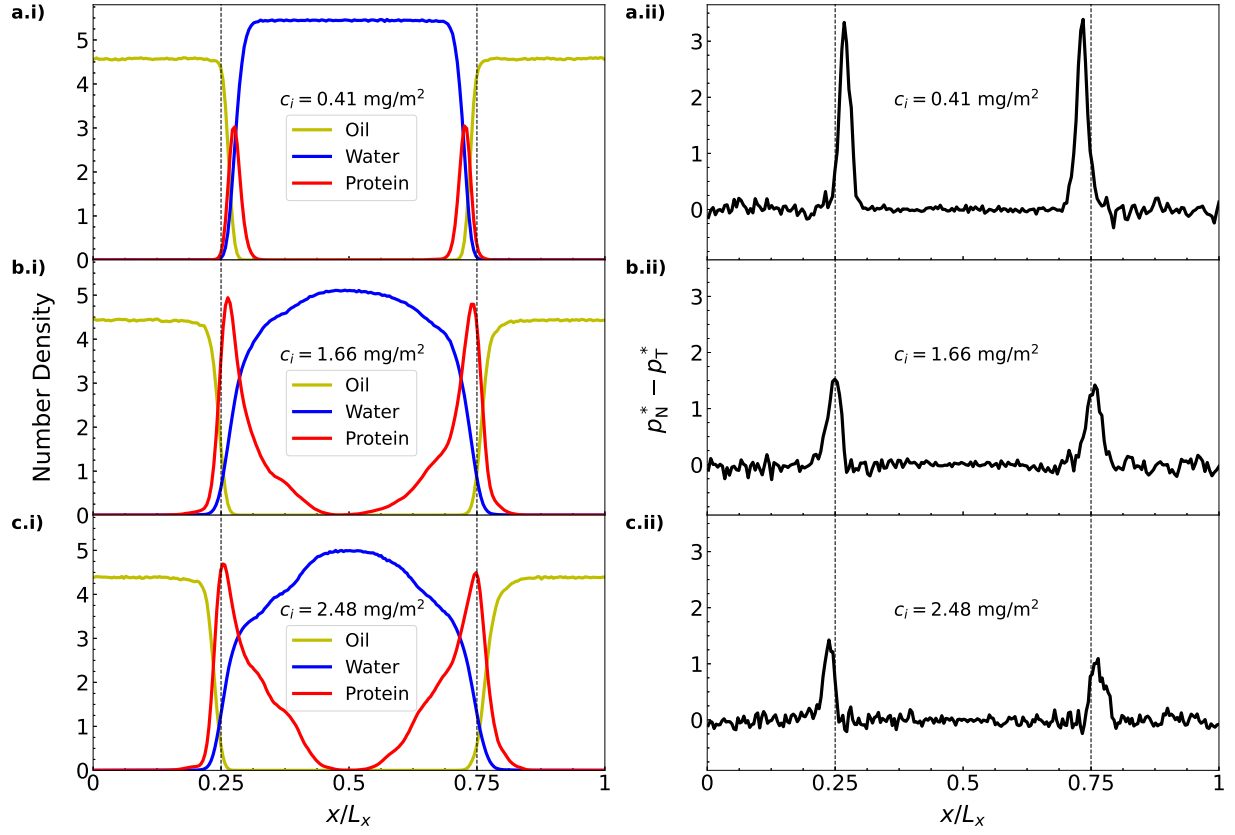
This is the author's peer reviewed, accepted manuscript. However, the online version of record will be different from this version once it has been copyedited and typeset.

PLEASE CITE THIS ARTICLE AS DOI: 10.1063/1.50079883



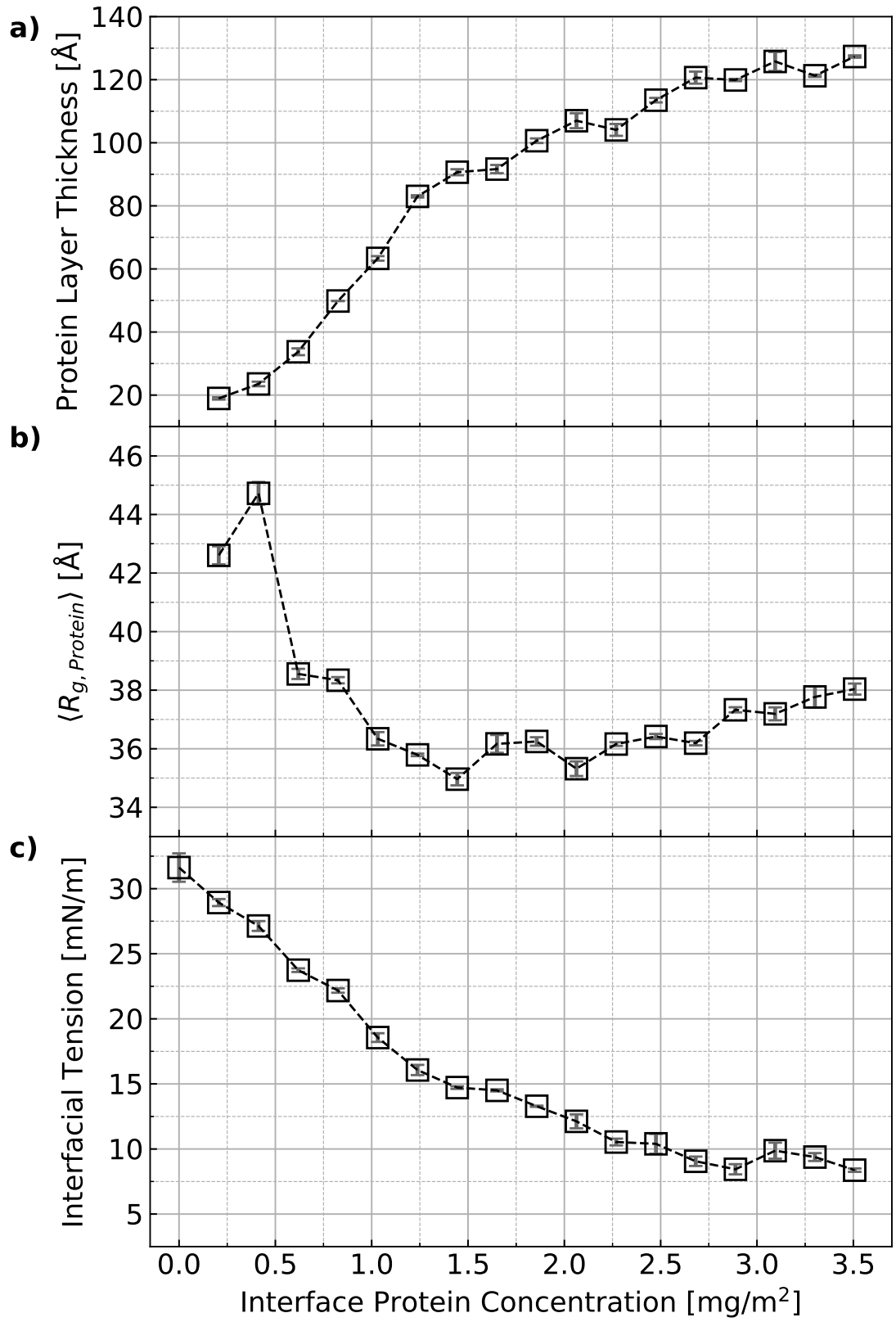
This is the author's peer reviewed, accepted manuscript. However, the online version of record will be different from this version once it has been copyedited and typeset.

PLEASE CITE THIS ARTICLE AS DOI: 10.1063/1.50079883



This is the author's peer reviewed, accepted manuscript. However, the online version of record will be different from this version once it has been copyedited and typeset.

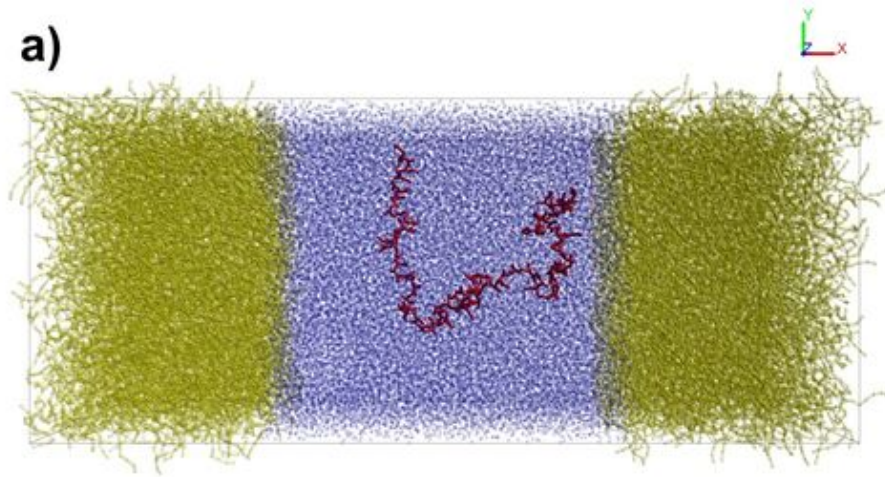
PLEASE CITE THIS ARTICLE AS DOI: 10.1063/5.0079883



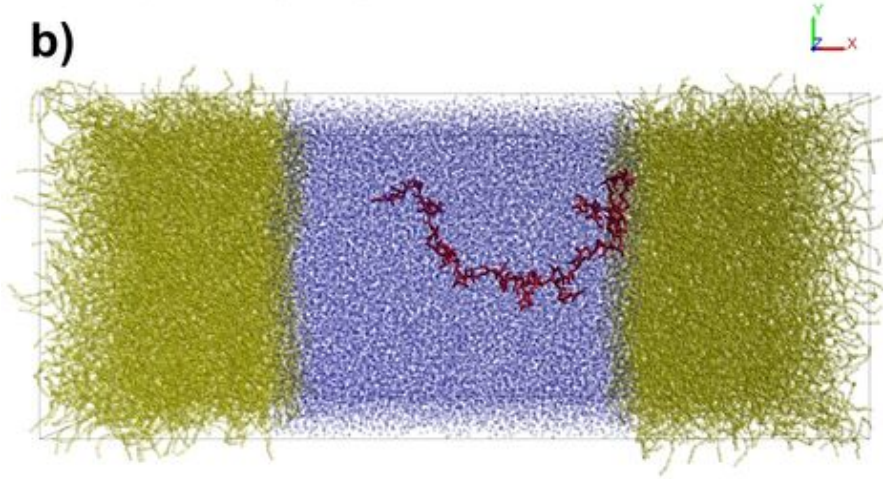


This is the author's peer reviewed, accepted manuscript. However, the online version of record will be different from this version once it has been copyedited and typeset.

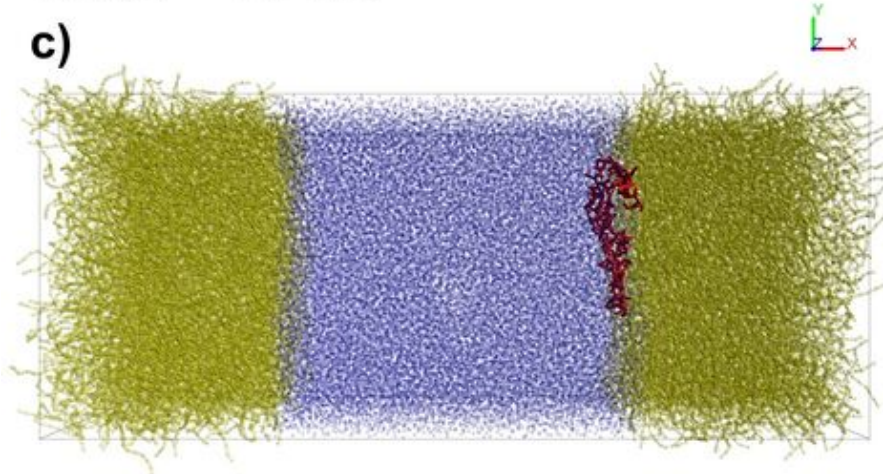
PLEASE CITE THIS ARTICLE AS DOI: 10.1063/1.50079883



**Time = 10 ns**



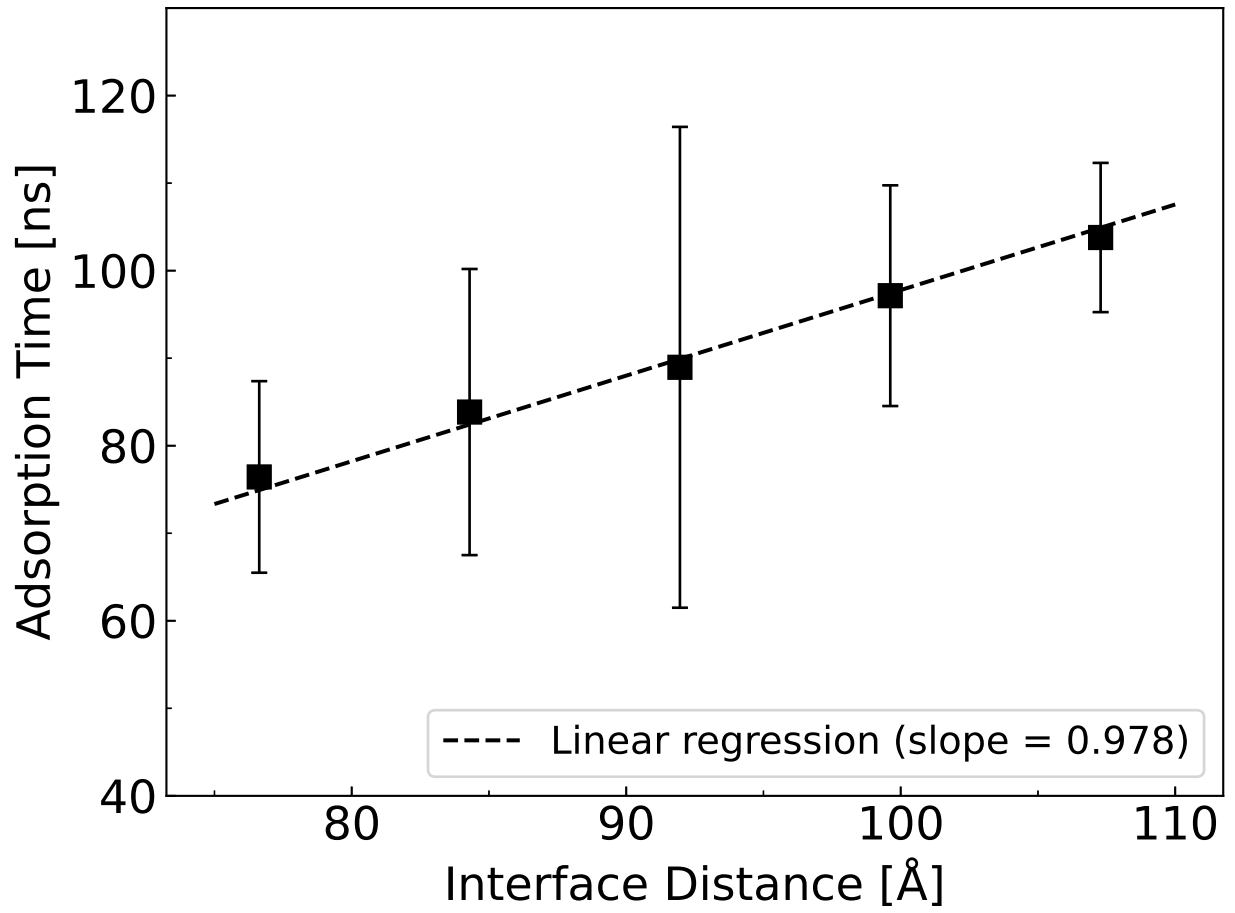
**Time = 20 ns**



**Time = 80 ns**

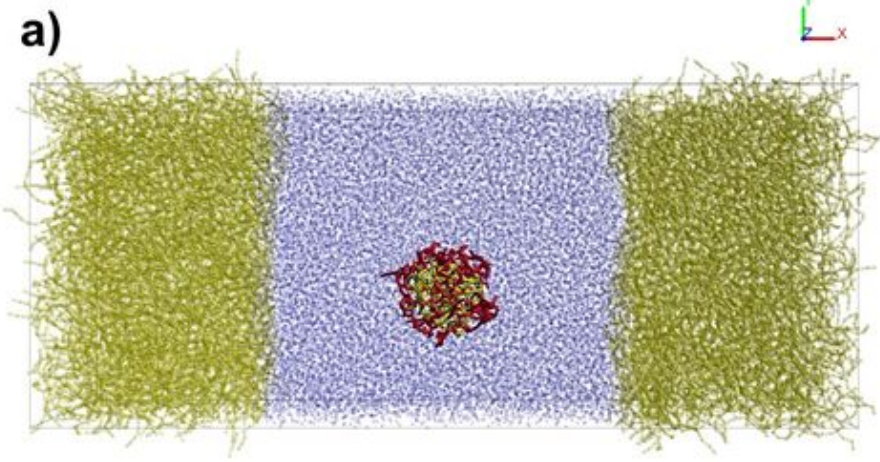
This is the author's peer reviewed, accepted manuscript. However, the online version of record will be different from this version once it has been copyedited and typeset.

PLEASE CITE THIS ARTICLE AS DOI: 10.1063/5.0079883

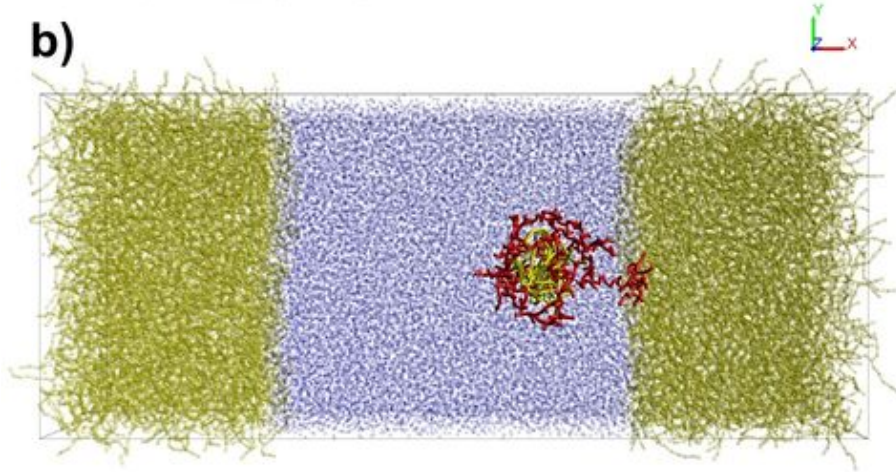


This is the author's peer reviewed, accepted manuscript. However, the online version of record will be different from this version once it has been copyedited and typeset.

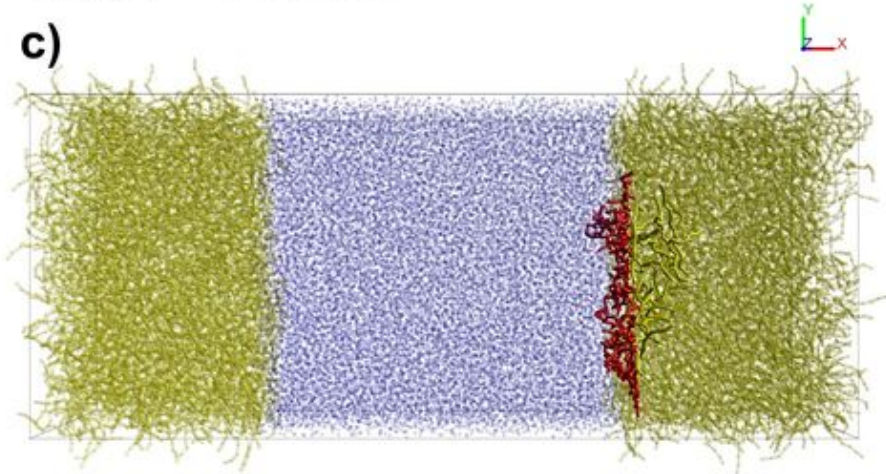
PLEASE CITE THIS ARTICLE AS DOI: 10.1063/1.50079883



**Time = 20 ns**



**Time = 230 ns**



**Time = 260 ns**